Biogeochemistry (2012) 110:215–241
DOI 10.1007/s10533-011-9648-1

DMS dynamics in the most oligotrophic subtropical zones of the global ocean

Sauveur Belviso · Italo Masotti · Alessandro Tagliabue · Laurent Bopp · P. Brockmann · Cédric Fichot · Guy Caniaux · Louis Prieur · Joséphine Ras · Julia Uitz · Hubert Loisel · David Dessailly · Séverine Alvain · Nobue Kasamatsu · Mitsuo Fukuchi

Received: 17 March 2011 / Accepted: 13 August 2011 / Published online: 24 September 2011

Abstract The influences of physico-chemical and biological processes on dimethylsulfide (DMS) dynamics in the most oligotrophic subtropical zones of the global ocean were investigated. As metrics for the dynamics of DMS and the so-called 'summer DMS paradox' of elevated summer concentrations when surface chlorophyll *a* (Chl) and particulate organic carbon (POC) levels are lowest, we used the DMS-to-Chl and DMS-to-POC ratios in the context of three independent and complementary approaches. Firstly, field observations of environmental variables (such as the solar radiation dose, phosphorus limitation of phytoplankton and bacterial growth) were used alongside discrete DMS, Chl and POC estimates extracted from global climatologies (i.e., a 'station based' approach). We then used monthly climatological data for DMS, Chl, and POC averaged over the biogeographic province wherein a given oligotrophic subtropical zone resides (i.e., a 'province based'

S. Belviso (✉) · I. Masotti · A. Tagliabue · L. Bopp · P. Brockmann
IPSL/Laboratoire des Sciences du Climat et de l'Environnement, CEA/CNRS/UVSQ, UMR 8212, CEN Saclay, Bât 701 l'Orme des Merisiers, 91191 Gif-sur-Yvette, France
e-mail: Sauveur.Belviso@lsce.ipsl.fr

Present Address:
A. Tagliabue
Department of Oceanography, University of Cape Town, Cape Town 7701, South Africa

C. Fichot
Marine Sciences Program, University of South Carolina Columbia, Columbia, SC 29208, USA

G. Caniaux
CNRM, GAME, Météo France, CNRS, 42 Avenue G. Coriolis, 31057 Toulouse Cedex, France

L. Prieur · J. Ras · J. Uitz
Laboratoire d'Océanographie de Villefranche, Université Pierre et Marie Curie, CNRS, UMR 7093, 06238 Villefranche-sur-mer Cedex, France

Present Address:
J. Uitz
Marine Physical Lab., Scripps Institution of Oceanography, University of California San Diego, 9500 Gilman Drive, La Jolla, CA 92093-0238, USA

H. Loisel · D. Dessailly · S. Alvain
Laboratoire d' Océanologie et de Géosciences, Université Lille Nord de France, UMR 8187, 62930 Wimereux, France

N. Kasamatsu · M. Fukuchi
National Institute of Polar Research, Research Organization of Information and Systems, 1-9-10 Kaga, Itabashi 173-8515, Japan

Present Address:
N. Kasamatsu
Tokyo University of Marine Science and Technology, 4-5-7 Konan, Minato-ku, Tokyo 108-8477, Japan

approach). Finally we employed sensitivity experiments with a new DMS module coupled to the ocean general circulation and biogeochemistry model PISCES to examine the influence of various processes in governing DMS dynamics in oligotrophic regions (i.e., a 'model based' approach). We find that the 'station based' and 'province based' approaches yield markedly different results. Interestingly, the 'province based' approach suggests the presence of a 'summer DMS paradox' in most all of the oligotrophic regions we studied. In contrast, the 'station based' approach suggests that the 'summer DMS paradox' is only present in the Sargasso Sea and eastern Mediterranean. Overall, we found the regional differences in the absolute and relative concentrations of DMS between 5 of the most oligotrophic regions of the world's oceans were better accounted for by their nutrient dynamics (specifically phosphorus limitation) than by physical factors often invoked, e.g., the solar radiation dose. Our 'model based' experiments suggest that it is the limitation of phytoplankton/bacterial production and bacterial consumption of DMS by pervasive phosphorus limitation that is responsible for the 'summer DMS paradox'.

Keywords Dimethylsulfide (DMS) · Oligotrophy · Summer DMS paradox · Modelling · Field observations

Introduction

Dimethylsulfide (DMS) is the predominant volatile sulfur compound in open ocean waters (Andreae 1990) and an important source of aerosol particles in the marine atmosphere (Vogt and Liss 2009) and references therein; Langley et al. 2010) that could affect cloud albedo and lifetime. As such, a better knowledge of the global distribution of DMS in the surface ocean is required. DMS is a product of dimethylsulfoniopropionate (DMSP) catabolism which involves different enzymatic pathways, not all well understood as yet (Todd et al. 2007). Since the early nineties, different approaches have been employed to understand the global distribution of DMS. The attempts made to compare seawater DMS concentrations either with particular oceanic properties (e.g., sea surface temperature (SST), mixed layer depth (MLD), solar irradiance, nutrients, chlorophyll *a* (Chl) or DMSP concentrations) or combinations of several variables, have met with mixed success (Andreae 1990; Kettle et al. 1999; Lana et al. 2011). Although the seasonality in DMS is certainly determined by the interplay between numerous physical and biogeochemical processes and parameters (Stefels et al. 2007), the most recent correlation analysis shows that the monthly ocean surface DMS distribution follows the average solar radiation intensity experienced by phytoplankton in the mixed layer (i.e., the surface radiation dose (SRD)) more closely than it follows SST, Chl or nutrient concentrations (Lana et al. (2011) after Vallina and Simó (2007)). Re-examination of the DMS-SRD relationship at a global scale by Derevianko et al. (2009), seems however to indicate that when using minimal aggregation methods, SRD accounts for only a small fraction (4–14%) of the total variance in DMS concentrations. At local scales, data show that DMS and SRD can be strongly correlated (Vallina and Simó 2007), but slopes and intercepts display little consistency in the Atlantic Ocean and adjacent seas (Archer et al. 2009; Belviso and Caniaux 2009; Miles et al. 2009). As shown by Belviso and Caniaux (2009), part of the discrepancy arises from the way in which SRDs are calculated. So, in order to investigate the spatial variations in DMS/SRD slopes, it is crucial to calculate SRDs in an identical fashion.

In the Sargasso Sea and in the north-western Mediterranean Sea, DMS concentrations and SRDs peak in summer (Dacey et al. 1998; Vallina and Simó 2007). On the other hand, in the north-eastern Atlantic Ocean off Portugal and in the western English Channel, DMS levels are markedly higher in spring than in summer (Archer et al. 2009; Belviso and Caniaux 2009). Since DMS concentrations and SRDs have not been monitored concomitantly apart from in the Atlantic and the Mediterranean Sea, there is not sufficient experimental evidence to demonstrate unequivocally that variations in biological factors are small enough for SRD to be dominant at local scales (as suggested by Derevianko et al. 2009). Based on the high correlation between DMS and SRD in the Sargasso Sea, it is expected that other oligotrophic subtropical zones of the global ocean would display similarly high DMS surface levels during the summer months. The cores of subtropical anticyclonic gyres are characterized by their oligotrophic status and minimal Chl concentration, compared to that of the

world ocean (Morel et al. 2010 and references therein). Not only the low Chl level, but also a reduced amount of colored dissolved organic matter (CDOM) account for the extreme clarity of waters. Although they may be similar, different oligotrophic zones are not identical regarding their Chl and CDOM contents, or their seasonal cycles (Morel et al. 2010). In spite of its low Chl, the Sargasso Sea presents the highest CDOM content amongst the six zones studied by these authors.

The existence of elevated summer DMS concentrations months after surface Chl levels have peaked has been termed as the 'summer DMS paradox' (Simó and Pedrós-Alió 1999). Here we use 3 different approaches to explore similarities and differences in terms of 'summer DMS paradox' between oligotrophic subtropical zones. One is a 'station based' analysis. To investigate whether the temporal variability in DMS concentration is explained by changes in SRD at some location, while its spatial variability is controlled by other factors, we assembled a database of SRDs, sea surface DMS concentrations and biogeochemical variables at or in the vicinity of the oligotrophic zones (Table 1) selected by Morel and Gentili (2009) and Morel et al. (2010). Next comes a 'province based' analysis using climatology products averaged over biogeographic provinces wherein oligotrophic regions reside. Finally a 'model based' approach is also used to examine the influence of various processes in governing DMS dynamics in oligotrophic regions.

Data and methods

The 'station based' approach

Overview of the selected geographic zones

We considered the six quadrangular domains selected by Morel et al. (2010), and used for comparison a mesotrophic site off Portugal (site P, see Table 1 and Fig. 1) which exhibits seasonal oligotrophy in summer as area S-ext. (see below), as well as a sub-zone in the oriental basin of the Mediterranean Sea coinciding with the most oligotrophic waters (Morel and Gentili

Table 1 Geographical information for the ten zones selected for the present study (see also map in Fig. 1); in addition are included the Longhurst's division of the oceans into static biogeographic provinces, as well as the number of DMS data in each location (data taken from the Global Surface Seawater DMS Database)

Location	Notation	Longitude		Latitude		Biogeographic provinces Acronym and reference number[a]	Number of DMS data
N-Hemisphere							
Hawaii Islands zone	H[b]	−170	−150.9	10	18	NPTE (38)	232
Mariana Islands zone	M[b]	150	165.9	10	20	NPTW (35) and WARM (41)	7
South-Sargasso Sea	S[b]	−70	−45	22	27	NASW (6) and NATR (7)	48
North- and South-Sargasso Sea	S-ext.[c]	−66	−52	22	34	NASW (6) and NATR (7)	390
Eastern Mediterranean Sea	Md[c]	33	36	14	32	MEDI (16)	135
Atlantic off Portugal	P[b]	−25	−15	34	40	NASE (18)	241
S-Hemisphere							
South Indian gyre	I[b]	70	90	−30	−21	ISSG (23)	0
Brasilian Atlantic gyre	B[b]	−32	−25.9	−22.5	−12.5	SATL (10)	157
Easter Island zone	E[b]	−125	−100	−30	−20	SPSG (37)	25
Easter Island extended zone	E-ext.[c]	−150	−100	−30	−20	SPSG (37)	192

The locations of the PROSOPE, POMME and BIOSOPE cruises, as well as the sampling stations BATS and Hydrostation S, are in areas denoted Md, P, E and S-ext., respectively

NPTE N. Pacific Tropical Gyre (East); *NPTW* N. Pacific Tropical Gyre (West); *WARM* W. Pacific Warm Pool; *NASW* N. Atlantic Subtropical Gyre (West); *NATR* N. Atlantic Tropical Gyre; *MEDI* Mediterranean Sea, Black Sea; *NASE* N. Atlantic Subtropical Gyre(East); *ISSG* Indian S. Subtropical Gyre; *SATL* South Atlantic Gyre; *SPSG* S. Pacific Subtropical Gyre

[a] Longhurst (1998) and Lana et al. (2011)

[b] Morel et al. (2010)

[c] This work

2009; denoted Md in Fig. 1). The latter was also spatially homogeneous in terms of CDOM absorption of UV radiation at 320 nm (the influence of the Nile river was discarded as well as that of other coastal waters). Unfortunately, there are few DMS measurements in the deep blue waters characterizing area S (Table 1), whereas the BATS station, located in the northern Sargasso Sea (Fig. 1), is a reference site for DMS experimentalists. That is why we selected a new quadrangular domain encompassing the BATS station (Fig. 1, white dotted contours). It is denoted S-ext. in Table 1 where ext. stands for 'extended area'. A similar approach was applied to the area E located in the South Pacific gyre in the vicinity of Easter Island (Table 1; Fig. 1). The new area (E-ext.) extends in longitude between 100°W and 150°W.

Similarities and differences in terms of climatological annual cycles of Chl and POC concentrations between Morel et al. (2010)'s areas and the two new ones are evaluated in Fig. 2. The seasonality in Chl and POC concentrations is not significantly affected by the longitudinal extension of area E. In the Atlantic Ocean, conversely, the latitudinal extension and longitudinal restriction strongly affect both variables. Area S-ext. does not exhibit permanent oligotrophy. However, the differences between the two areas are much less marked during the summer months (J, Ju, A, and S) than in winter. In other words, both areas S and S-ext. exhibit spatial and temporal homogeneity in terms of oligotrophic conditions during the summer period.

DMS, Chl and POC concentrations

We used discrete DMS measurements taken from the Global Surface Seawater DMS Database (http://saga.pmel.noaa.gov/dms/) and calculated monthly averages in each selected zone. Areas M and I are free of DMS data (Fig. 1). However, some DMS measurements were carried out west of the south-west corner of area M (Fig. 1). We arbitrarily allocated these measurements to area M. Chl and POC estimates were extracted from global climatologies (Table 2).

Physical and biogeochemical variables

We consider both the environmental and biogeochemical parameters that are likely to affect the production and removal of DMS, and the recently

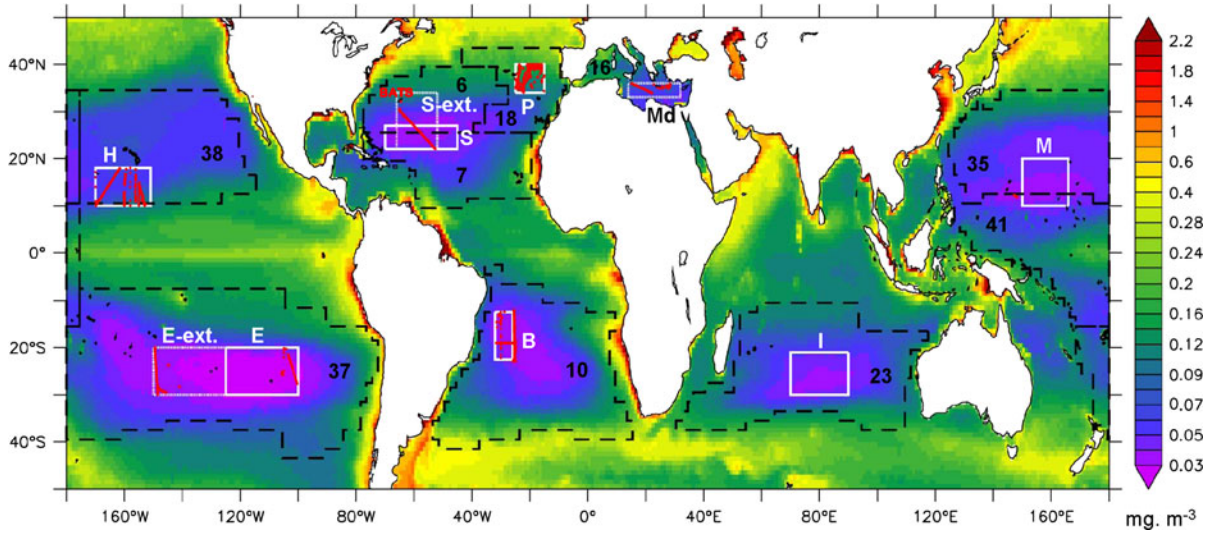

Fig. 1 Annual mean values of Chl concentration (1997–2010, in mg m^{-3}) for the global ocean. Following the procedure of Morel and Gentili (2009), SeaWiFS data were corrected for the presence of yellow substance (CDOM) in varying proportions with respect to Chl. The *solid white boxes* superimposed on the map show the six oligotrophic zones selected by Morel et al. (2010), i.e. S, H, E, B, I and M (see also Table 1 for the exact locations and meaning of the identifiers). The mesotrophic zone off Portugal (P) is selected for a comparison as in Morel et al. (2010). The *boxes with dotted-white* contours (i.e., S-ext., E-ext. and Md) were selected either to augment the number of DMS data identified with *red dots* in each box (S-ext. and E-ext.) or to exclude the coastal waters from the analysis in the narrow oriental basin of the Mediterranean Sea (Md). Also shown with *black dashed lines* are the ten Longhurst's static biogeographic provinces wherein a given oligotrophic subtropical zone resides. The meaning of the numbers is provided in Table 1

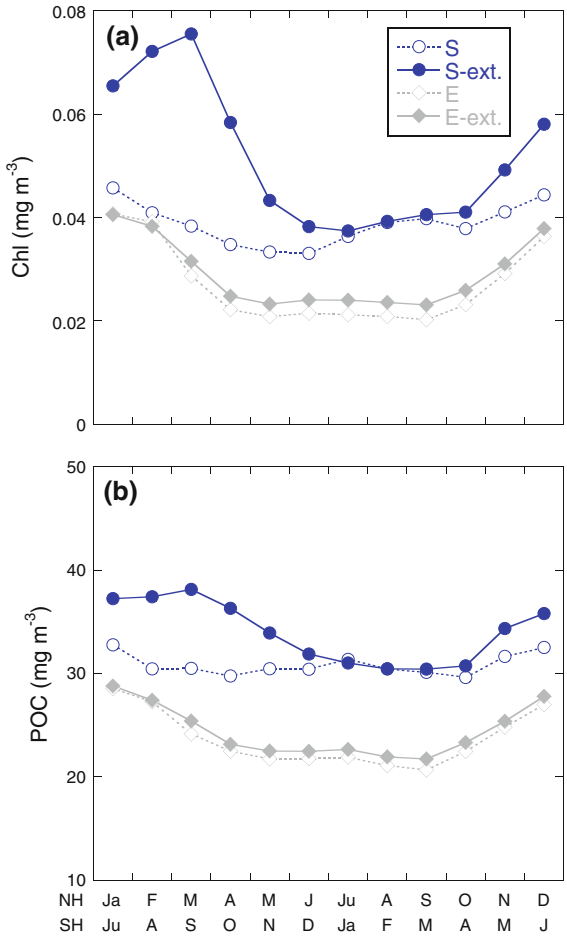

Fig. 2 Climatological annual cycles of averaged **a** Chl and **b** POC concentrations within the zones S, S-ext., E and E-ext. (see Table 1 for the exact locations and meaning of the identifiers). The month scale begins with January for the Northern Hemisphere and in July for the Southern Hemisphere

proposed notion of mixed layer solar radiation dose (SRD).

Standardization procedure for SRD estimates In order to evaluate the average solar radiation intensity experienced by phytoplankton in the mixed layer, Vallina and Simó (2007) defined the daily-average solar radiation dose (SRD) by:

$$\mathrm{SRD} = \frac{1}{\mathrm{MLD}} \int_0^{\mathrm{MLD}} I(z)dz \qquad (1)$$

where MLD is the mixed layer depth (units in m) and $I(z)$ the irradiance (W m^{-2}) at depth z. The MLD is defined as the depth at which the temperature is 0.1°C lower than that at 5 m depth (Vallina and Simó 2007; Miles et al. 2009; Derevianko et al. 2009). For the decay of the solar irradiance with depth, Vallina and Simó (2007) considered an exponential law of the Beer–Lambert form:

$$I(z) = I_0 \exp(-kz) \qquad (2)$$

where k is the diffuse attenuation coefficient (units m^{-1}) and I_0 the incident solar irradiance. Only one exponential was used in Eq. 2 because the authors were right in what they were assuming that DMS production was not dependent on the infrared radiation but on the visible part of the solar radiation available for phytoplankton growth. However, it is well established in the literature that DMS production and consumption by phytoplankton and bacteria also respond to UV radiation dose (e.g., Sunda et al. 2002; Toole and Siegel 2004). Here both PAR and UV doses will be taken into account but treated independently.

Standardization procedure for SRD estimates in the PAR domain. We believe that the intensity of SRD determined by Vallina and Simó (2007) and several authors (Miles et al. 2009; Derevianko et al. 2009; Belviso and Caniaux 2009) is largely over-estimated (Tables 3, 4). This can lead to ambiguous comparisons when applied at different locations of the global ocean and finally to divergent analyses when regressed with DMS measurements. This overestimation is due to two factors: (i) I_0 is generally measured above the sea surface by pyranometers covering the global solar radiation spectrum (300–3000 nm) instead of the photosynthetically available radiation (PAR, 300–700 nm), which constitutes only 40% of the total irradiance at the Earth's surface (Jerlov 1974; Jitts et al. 1976); (ii) I_0 has to take account the reflection at sea surface. Classical reflection coefficient values of 0.06 are reported (Payne 1972; Katsaros et al. 1985) and used here.

For these reasons, we use the following expression for computing the SRD:

$$\mathrm{SRD} = \frac{1}{\mathrm{MLD}} \int_0^{\mathrm{MLD}} (1-\alpha) I\downarrow \exp(-kz)dz \qquad (3)$$

where α is the reflection coefficient (0.06) and $I\downarrow$ the PAR (i.e. 43% the total solar irradiance). In agreement

Table 2 Similarities and differences in terms of physical, chemical and biological variables between the different oligotrophic subtropical zones investigated during summer

Variables	Data sources and references	Location and months					Figure number this work
		Md Ju, S	P A, S	E-ext. D, Ja	E-ext. F, M	B F, M	
DMS	DMS database: http://saga.pmel.noaa.gov/dms/	~	− −	− −	− −	− −	5a
DMS/Chl	DMS database: http://saga.pmel.noaa.gov/dms/	~	− −	− −	~	− −	5b
	Corrected Chl climatology (Morel et al. 2010)						
DMS/POC	DMS database: http://saga.pmel.noaa.gov/dms/	~	− −	− −	~	− −	5c
	POC climatology (Duforêt-Gaurier et al. 2010)						
Ventilation to atmosphere (DMS sea-to-air transfer velocity: kg)	SST and wind speed climatologies: http://jisao.washington.edu/data/coads_climatologies/	~	~	~	~	~	6b
	Sc number: Saltzman et al. (1993), kg: Wanninkhof (1992)						
Surface water stratification	MLD climatology (Kara et al. 2003)	~	~	− −	− −	− −	6a
UV photon absorption rate	MLD climatology (Kara et al. 2003)	~	~	~	~	~	6d
Photochemical potential	UV downward irradiance (Ruggaber et al. 1994)						
	Diffuse attenuation coefficient (Fichot et al. 2008)						
	Absorption coefficient of CDOM (Fichot and Miller 2010)						
Phytoplankton group dominance[a]	PHYSAT (Alvain et al. 2008)	PRO or NANO	PRO or NANO	SYN[f]	SYN[f]	SYN	8
Phytoplankton pigment-based size classes[b]	Pigment database (Uitz et al. 2006)	PICO & NANO	PICO	PICO	nd	nd	7c–e
Mixed layer UV dose(UV stress)	MLD climatology (Kara et al. 2003)	~	~	~	~	~	6c
	UV downward irradiance (Ruggaber et al. 1994)						
	Diffuse attenuation coefficient (Fichot et al. 2008)						
Photoprotection index	Pigment database (Uitz et al. 2006)	~	− −	~	nd	nd	7b
Limiting nutrient for phyto. and bacterial growth	DIP concentration[c] (Mather et al. 2008; Moutin et al. 2008)	~	++	++	++	++	_
	DIP turnover time[d] (Moutin et al. 2008)	− −	++	++	nd	nd	
	Limiting nutrient[e] (Moutin et al. 2008; Van Wambeke et al. 2002, 2008)	P	nd	N	nd	nd	

The reference site is S-ext. Summer is J, Ju, A, S in the Northern Hemisphere and D, Ja, F, M is the Southern Hemisphere. Values in Md, P, E-ext. and B are at least twice higher (++) or at least twice lower (− −) than in S-ext.; if not (~)

nd no data

[a] The dominant phytoplankton group in area S-ext. is PRO but NANO or COC dominance is also detected during summer (Fig. 8a)

[b] The dominant phytoplankton pigment-based size class in area S-ext. is nanophytoplankton (Fig. 7d)

[c] In summer in S-ext., [DIP] is 2–5 nM (Lomas et al. 2010)

[d] DIP turnover time is 5 h (Cotner et al. 1997). The limiting nutrient is P (Wu et al. 2000)

[e] From enrichment experiments

[f] But unidentified pixels cover about half of the investigated area

Table 3 Statistics concerning SRD and DMS/SRD relationship in the literature (local scale)

Location	SRD (W m^{-2})	N	Slope	r^2	ρ	References
Northwestern Med. Sea	10–290	15	0.028	0.94	0.75	Vallina and Simó (2007)
Blanes Bay						
Bermuda Hydrostation S	5–230	33	0.017	0.81	0.89	Vallina and Simó (2007)
POMME cruises[a]	0–90	232	0.051	0.19	0.74	Belviso and Caniaux (2009)
AMT cruises[b]						
In situ data	0–220	65	0.006	–	0.55	Miles et al. (2009)
Climatology	20–210	65	0.010		0.74	
English Channel Station L4	0–55	33	0.13	0.25	–	Archer et al. (2009)

Column 2 is the range of SRD values; N the number of samples used; Slope, r^2 and ρ are respectively the slope, the coefficient of determination and the Spearman rank correlation coefficient of the DMS/SRD regression. More details available in Table 4

[a] Northeast Atlantic Ocean (39°N–44.5°N, 16.5°W–21°W)

[b] Atlantic Ocean (45°N–40°S, roughly along 30°W)

Table 4 List of data sources and methods for calculating SRD in the literature

Location	$I(z)$	MLD	k	References
Blanes Bay	Pyranometer; one exponential	CTD; 0.2°C and 0 m	PAR	Vallina and Simó (2007)
Bermuda Hydrostation S	Pyranometer; one exponential	CTD BATS; 0.1°C and 5 m	Z_e (PAR from BATS)	Vallina and Simó (2007)
Global Ocean	0.5 * I_{ToA} (computed from a model); one exponential	BM04; 0.1°C and 5 m	0.06 m^{-1}	Vallina and Simó (2007)
POMME	Pyranometer (300–2800 nm) and satellite retrievals; one and two exponentials	CTD; several criteria including 0.1°C and 5 m	D1 and D2 from Jerlov (1977)	Belviso and Caniaux (2009)
AMT	Pyranometer (300–3000 nm); one exponential	CTD at 03 h LT; 0.1°C and 5 m	Z_e at 11 h LT	Miles et al. (2009)
English Channel Station L4	ELDONET dosimeter; (400–700 nm)	CTD; 0.8°C and 0 m	PAR	Archer et al. (2009)
Global Ocean	ISCCP surface solar irradiance; one exponential	BM04; 0.2°C and 10 m	0.06 m^{-1}	Derevianko et al. (2009)

$I(z)$ refer to the solar irradiance decay in the water column; MLD stands for the mixed layer depth and k the light extinction coefficient. BM04 refers to the de Boyer Montégut et al. (2004) climatology

with Vallina and Simó (2007) and Miles et al. (2009), k, the diffuse attenuation coefficient, can be determined from underwater PAR measurements (i.e. $k = 4.605/Z_e$, where Z_e is the euphotic depth, at which 99% of the underwater PAR attenuates). Integrating Eq. 3 over the MLD, with k now constant with depth, leads to:

$$\mathrm{SRD} = \frac{(1-\alpha)I\downarrow}{k\mathrm{MLD}}\{1-\exp(-k\mathrm{MLD})\} \quad (4)$$

Using this expression, the SRD values from the data sets considered in this study can be compared as if they were estimated similarly, despite their different origin. In Table 5, some details are given on the data sets used for calculating SRD from Eq. 4. The cruises PROSOPE, BIOSOPE and POMME were carried out in the Mediterranean Sea, in the South Pacific gyre and in the north-eastern Atlantic Ocean off Portugal, respectively. BATS is the Bermuda Atlantic Time-Series Study station. The DMS measurements were obtained during those studies or as close as possible to those locations (both geographically and temporally).

During PROSOPE, atmospheric PAR was measured on the ship instead of global incident irradiance

Table 5 List of input parameters, method and criteria used for the calculation of SRD

Experiment	N	MLD	Surface irradiance	k method
BATS (summers 1992–1994)	41	CTD 0.1° and 5 m	Pyranometer	Z_e from Chl a profiles at some spots
PROSOPE (1999)	51	CTD 0.1° and 5 m	PAR	Z_e from underwater PAR profiles at some spots
BIOSOPE (2004)	218	CTD 0.1° and 5 m	Pyranometer	Z_e from underwater PAR profiles at some spots
POMME (2001)	232	CTD 0.1° and 5 m	Pyranometer	Z_e from Chl a profiles at each CTD cast

N is the number of CTDs used, k the light extinction coefficient. However, only a fraction of the PROSOPE, BIOSOPE and POMME data sets was used since our study is restricted temporally (summer months only i.e. cruise POMME 3 carried out in September 2001), and spatially (oligotrophic areas: site MIO during PROSOPE, and stations 9–12 during cruise BIOSOPE)

(motivating the use of the 0.43 factor for the other data sets). For POMME and BATS, k was determined from Chl profiles (unit mg m^{-3}) using the following expressions (Morel and Berthon 1989):

$$Z_e = 568.2\left\langle \int_0^{Z_e} (\mathrm{Chl})dz \right\rangle^{-0.746} \quad \text{when } Z_e < 102\,\mathrm{m}$$

and

$$Z_e = 200\left\langle \int_0^{Z_e} (\mathrm{Chl})dz \right\rangle^{-0.293} \quad \text{when } Z_e > 102\,\mathrm{m} \tag{5}$$

Then k and SRD were calculated for each CTD by using the nearest time Z_e value. During BIOSOPE and PROSOPE, PAR profiles were only collected at some stops of the ship and consequently Z_e values were calculated from these profiles and k and SRD determined for each CTD by using the nearest Z_e value.

Standardization procedure for SRD estimates in the UV domain. Monthly climatologies of the average incident UV downward scalar irradiance in the mixed layer, SRD(UV) (mol(photons) m^{-2} day^{-1}), was estimated for the studied regions using Eq. 6:

$$\mathrm{SRD(UV)} \approx \frac{1}{\mathrm{MLD}} \int_0^{\mathrm{MLD}} \int_{\lambda_1}^{\lambda_2} E_{\mathrm{od}}(\lambda, 0^-) e^{-K_d(\lambda)z} \mathrm{d}\lambda \mathrm{d}z \tag{6}$$

where $E_{\mathrm{od}}(\lambda, 0^-)$ is the scalar downward irradiance just below sea surface (mol(photons) m^{-2} day^{-1} nm^{-1}), and $K_d(\lambda)$ is the average diffuse attenuation coefficient of downwelling irradiance for the mixed layer (m^{-1}). SRD(UV) was computed for the combined UV-B/UV-A region (290–400 nm).

The monthly climatologies of MLD, $E_{\mathrm{od}}(\lambda, 0^-)$, and $K_d(\lambda)$ used in the calculations are described in detail in Fichot and Miller (2010) along with a discussion about uncertainties associated with assumptions made in the modeling. Note that a spectral resolution of 2-nm was used in the present work, in contrast to the 5-nm spectral resolution used in Fichot and Miller (2010). For each region studied, SRD(UV) was first calculated for the individual elements of the spatial grid corresponding to the region. Then, the spatial average and standard deviation for each region was computed.

Note that SRD(UV) are expressed here in units of mol(photons) m^{-2} day^{-1} whereas SRD in the PAR domain are expressed in units of W m^{-2}. There are two main reasons for this discrepancy: 1) SRD(PAR) are calculated here from broadband radiometric measurements for which a conversion to quantum units can lead to significant errors because some assumption on the spectral characteristics of the incident irradiance is required; 2) the absorption of a photon is the fundamental process in photochemical reactions such that SRD(UV) (modeled here from spectrally resolved data) are best expressed in quantum units when investigating the role of UV radiation on DMS dynamics.

Biogeochemical variables relevant for the marine sulfur cycle Phytoplankton group dominance, phytoplankton pigment-based size classes, photoprotection index, mixed layer UV photon absorption rate by CDOM together with dissolved inorganic phosphorus (DIP) concentrations and turnover times (a measure of phosphate limitation which can also be assessed from enrichment experiments), were gathered from several databases, from computed climatologies and from the

literature (Table 2 and associated references). The first three variables are relevant for the DMS cycle because algal composition and the physiological conditions of the algal cells affect DMSP and DMS production (Stefels et al. 2007). Light and nutrient stresses are also potentially important factors controlling bacterial consumption of DMSP and DMS (Polimene et al. this issue). Concerning the UV absorption by CDOM, a potential source of free radicals likely involved in the photo-oxidation of DMS (Toole and Siegel 2004), monthly climatologies of the average UV photon absorption rate in the mixed layer, $\Xi^{\mathrm{MLD}}(\mathrm{UV})$ (mol(photons) m^{-2} day^{-1}), were estimated for the studied regions using Eq. 7:

$$\Xi^{\mathrm{MLD}}(\mathrm{UV}) \approx \frac{1}{\mathrm{MLD}} \int_0^{\mathrm{MLD}} \int_{\lambda_1}^{\lambda_2} E_{\mathrm{od}}(\lambda, 0^-) e^{-K_{\mathrm{d}}(\lambda) z} a_{\mathrm{g}}(\lambda) \mathrm{d}\lambda \mathrm{d}z, \quad (7)$$

where $a_{\mathrm{g}}(\lambda)$ is the average absorption coefficient of CDOM for the mixed layer (m^{-1}). $\Xi^{\mathrm{MLD}}(\mathrm{UV})$ was computed for the combined UV-B/UV-A region. The monthly climatologies of $a_{\mathrm{g}}(\lambda)$ used in the calculations are described in detail in Fichot and Miller (2010) along with a discussion of uncertainties associated with assumptions made in the modeling. A spectral resolution of 2-nm was used in the present work, in contrast to the 5-nm spectral resolution used in Fichot and Miller (2010). For each region studied, $\Xi^{\mathrm{MLD}}(\mathrm{UV})$ was first calculated for the individual elements of the spatial grid corresponding to the region. Then, the spatial average and standard deviation for each region was computed.

The 'province based' approach

The climatology of Kettle et al. (1999), recently updated by Lana et al. (2011), uses interpolation/extrapolation techniques that are applied to project the discrete DMS surface concentration data onto a first guess field based on Longhurst's biogeographic provinces. Further objective analysis allows the authors to obtain the final monthly climatological maps. Figure 1 displays the Longhurst (1998) divisions of the subtropical oceans into static biogeographic provinces. Hence, we used monthly climatological data for DMS, Chl, and POC averaged over the biogeographic province wherein a given oligotrophic subtropical zone resides (Table 1).

The 'model based' approach

The PISCES model

PISCES (acronym for "Pelagic Interaction Scheme for Carbon and Ecosystem Studies") is a biogeochemical model (Aumont and Bopp 2006), which simulates marine biological production and describes the cycles of carbon and of the main nutrients (phosphate, nitrate, ammonium, iron and silicate). Two phytoplankton functional groups (nanophytoplankton and diatoms which are of central importance in the biogeochemical cycles of sulfur and carbon, respectively) and two zooplankton functional groups (mesozooplankton and microzooplankton), as well as two detrital size classes are also represented. PISCES is embedded within the global general ocean circulation model NEMO (Madec et al. 1998). PISCES was designed to be used over a wide range of spatial and temporal scales. A complete description of PISCES can be found in Aumont and Bopp (2006) and a release of the model is available to the community (http://www.nemo-ocean.eu/).

A new DMS module

The first prognostic module computing seawater DMS concentrations and DMS air–sea fluxes embedded within PISCES was developed by Bopp et al. (2008). This model was used to explore the relationship between iron fertilization and DMS production in the Southern Ocean. For the purposes of this study, which aims at investigating the dynamics of DMS in oligotrophic regions, we introduced a new parameterization into the DMS module. Most of the new equations were taken from the PlankTOM5 model (Vogt et al. 2010) which better captures the temporal decoupling between chlorophyll and DMS in poorly productive waters. This results in DMS concentrations that are highest several weeks after Chl concentrations have already peaked (e.g., Simó and Pedrós-Alió 1999). Here, we only describe the equations and parameters used in the DMS module.

The DMS module explicitly represents DMSP in the particulate form (pDMSP) and dissolved DMS according to the following equations:

$$\mathrm{pDMSP} = \sum_i \left(\frac{S}{C}\right)^i C_i, \tag{8}$$

$$\frac{\partial \mathrm{DMS}}{\partial t} = \sum_i [G_i + E_i + M_i] \left(\frac{S}{C}\right)^i Y_S - \lambda^*_{\mathrm{DMS}}\mathrm{DMS} - \lambda^{\mathrm{PAR}}_{\mathrm{DMS}} * \lambda^{\mathrm{NO_3}}_{\mathrm{DMS}} * \mathrm{DMS} - k_g\mathrm{DMS}, \tag{9}$$

where the subscript *i* represents the two phytoplankton groups in PISCES, i.e. diatoms and nanophytoplankton. The different terms of these two equations are described below.

In Eq. 8, pDMSP is computed from the carbon biomass of the two phytoplankton groups via group-specific sulfur (DMSP)-to-carbon (S/C) ratios (Stefels et al. 2007 and references therein). Recent studies have highlighted large variability in S/C ratios within a specific phytoplankton group as a function of environmental factors (e.g. Sunda et al. 2002; Bucciarelli and Sunda 2003). For nanophytoplankton and diatoms, we employ a variable S/C ratio that increases in response to nutrient, light and temperature stress. We use the equations for light (PAR), nutrient (Fe, DIP or PO_4) stress (S1, S2, S3, respectively), and temperature (T) dependence as proposed by Vogt et al. (2010) to simulate DMS in the PlankTOM5 model. The T dependence simulates the function of DMS and DMSP in cryoprotection (Karsten et al.1996). It has been set to enhance the S/C ratio for low temperatures, so mostly in polar waters. Hence, S/C ratio is described as

$$\left(\frac{S}{C}\right)^i = \left(\frac{S}{C}\right)^i_{\mathrm{min}} + \left(\frac{S}{C}\right)^i_{\mathrm{var}} * (\max(S1, S2, S3, 0.3) * 2 - f_{\mathrm{corr}}) * \left(1 + \frac{1}{(T+2.5)^6}\right) \tag{10}$$

where

$$S1 = \frac{\mathrm{PAR}}{\mathrm{PAR}_{\mathrm{max}}}, \tag{11}$$

$$S2 = \frac{K_{\mathrm{Fe}}}{\mathrm{Fe} + K_{\mathrm{Fe}}}, \tag{12}$$

$$S3 = 0.7 * \frac{K_{\mathrm{PO_4}}}{\mathrm{PO_4} + K_{E_4}}, \tag{13}$$

In Eq. 10, $\left(\frac{S}{C}\right)^i_{\mathrm{min}}$ and $\left(\frac{S}{C}\right)^i_{\mathrm{var}}$ are two parameters representing the minimum and the variable part of the S/C ratio for each phytoplankton. For example, diatom cultures show that the S/C ratio of *S. costatum* roughly doubles under nitrogen limitation (Sunda et al. 2007). The S/C ratio of the diatom *T. oceanica* roughly triples under Fe limitation (E. Bucciarelli. pers. com.). That is why we have introduced a variable part to the S/C ratio for diatoms as for nanophytoplankton (Bopp et al. 2008). The S/C ratio is assumed to adapt instantaneously to the local conditions as observations summarized in the review of Stefels et al. (2007) suggest. In Eq. 10, f_{corr} is an adjustable correction factor to tune global pDMSP concentration, currently set to 0.25 (Vogt et al. 2010). As the UV radiation level is not explicitly computed in PISCES, we assume that high PAR is associated with high UV levels in order to compute the S1 term in Eq. 11. In Eqs. 12 and 13 K_N are the phytoplankton half-saturation constants for nutrients (Fe and PO_4). The set of parameters used are summarized in Table 6. Hence, S/C can vary between 0.015 and 0.030 for nanophytoplankton, and between 0.0018 and 0.0036 for diatoms.

In Eq. 9, pDMSP is released to seawater as dissolved DMSP (dDMSP) via three different processes: 1) grazing by zooplankton (Gi), 2) exudation by phytoplankton (Ei), and 3) phytoplankton cell lysis (Mi). These terms are modeled as per Lefèvre et al. (2002): in short, all pDMSP grazed by zooplankton is released to seawater, the exudation of dDMSP is similar to that of dissolved organic matter (DOM), and the cell lysis is computed from phytoplankton mortality. The amount of DMSP released by these processes is proportional to the S/C cell ratio. Ron Kiene's main argument in 2000 was that dDMSP itself could be in short supply and so figure into the determination of DMS yields as dDMSP is broken down. Bacteria in need of sulfur would keep the sulfur-containing molecule, which then enters into DMSP catabolism via a demethylation pathway (Kiene et al. 2000). This core reasoning does not appear in our DMS module because we assume that, once released into water, dDMSP is instantaneously transformed into DMS by bacteria. We also assume that the dDMSP-to-DMS yield (the percentage of DMSP cleaved by DMSP lyases) is linked to bacterial activity. For instance, if bacterial activity is low due to nutrient limitation, the demethylation pathway is minor and DMS yield increases. The dDMSP-to-DMS yield varies both

Table 6 Model coefficients related to the DMS cycle with their standard values in PISCES, and references

Parameter	Unit	Value	Description	References
a	day^{-1}	0.66	Growth rate at 0°C for nanophyto., diatoms, and bacteria	Aumont and Bopp (2006)
b	–	1.066	Temperature sensitivity of growth	Aumont and Bopp (2006)
K_{PO_4}	µM P	0.001/0.004/ 0.0008	PO_4 half-saturation constants: nano/diatoms/ bacteria	Aumont and Bopp (2006)
K_{NH_4}	µM N	0.013/0.065/ 0.013	NH_4 half-saturation constants: nano/diatoms/ bacteria	Aumont and Bopp (2006)
K_{NO_3}	µM N	0.26/1.3	NO_3 half-saturation constants: nano/diatoms	Aumont and Bopp (2006)
K_{Si}	µM Si	2	Si half-saturation constant for diatoms	Aumont and Bopp (2006)
K_{Fe}	nM Fe	0.02/0.1/0.02	Minimum Fe half-saturation constant for: nano/diatoms/bacteria	Aumont and Bopp (2006)
K_{DOC}	µM C	5	DOC half-saturation constant for bacteria	Vogt et al. (2010)
$K_{DMS\text{-}bac}$	nM S	1.25	Half-saturation constant of DMS loss to bacterial consumption	Archer et al. (2002)
$(S/C)_{min\text{-}diato}$	mol S (mol C)$^{-1}$	0.0018	Minimum S-to-C ratio of diatoms	Stefels et al. (2007)
$(S/C)_{var\text{-}diato}$	mol S (mol C)$^{-1}$	0.0018	Variable S-to-C ratio of diatoms	This work
$(S/C)_{min\text{-}nano}$	mol S (mol C)$^{-1}$	0.015	Minimum S-to-C ratio of nanophytoplankton	Stefels et al. (2007)
$(S/C)_{var\text{-}nano}$	mol S (mol C)$^{-1}$	0.015	Variable S-to-C ratio of nanophytoplankton	This work
$Y_{S\ min}$	–	0.4	Minimum DMSP-to-DMS conversion yield	Vezina (2004)
$Y_{S\ var}$	–	0.2	Variable DMSP-to-DMS conversion yield	This work
λ^{B}_{DMS}	day^{-1}	0.2	DMS loss rate by bacterial activity	Kieber et al. (1996)
PAR_{max}	W m^{-2}	80	Maximal PAR	Vogt et al. (2010)
f_3	day^{-1}	0.25	Maximum rate of photolysis of DMS to DOC	Archer et al. (2004)
h1	W m^{-2}	5	Michaelis–Menten PAR limitation value	Archer et al. (2004)

Adapted from Bopp et al. (2008)

spatially and temporally in a very large range (Simó and Pedrós-Alió 1999). Vezina (2004) reported dDMSP-to-DMS yields in the range 18–68%. The following parameterization was adopted to estimate dDMSP-to-DMS yields (Y_S):

$$Y_S = Y_{S\,min} + Y_{S\,var} * \left(1 - L^B_{lim}\right), \quad (14)$$

$$L^B_{lim} = \min\left(L^B_{PO_4}, L^B_{Fe}, L^B_{DOC}\right), \quad (15)$$

where

$$L^B_x = [x]/(K_x + [x]),$$

In this set of equations, L^B_{lim} is the bacterial nutrient stress factor, and $Y_{S\ min}$ and $Y_{S\ var}$ are the minimum and the variable part of the dDMSP-to-DMS yield, respectively. In short, the modeled dDMSP-to-DMS yield increases from 40% to 60% as a function of the bacterial nutrient stress.

In seawater, DMS is lost due to bacterial (λ^*_{DMS}DMS) and photochemical ($\lambda^{PAR}_{DMS} * \lambda^{NO_3}_{DMS}$ *DMS) processes, and ventilation to the atmosphere (k_gDMS). The bacterial consumption of DMS is parameterized as a function of the bacterial biomass (B) and activity:

$$\lambda^{*}_{\mathrm{DMS}} = \lambda^{\mathrm{B}}_{\mathrm{DMS}} * L^{\mathrm{B}}_{\mathrm{lim-DMS}} * L^{\mathrm{B}}_{\mathrm{PAR}} * b^{\mathrm{T}} * \mathrm{B}_{\mathrm{DMS}} * \mathrm{B} \quad (16)$$

$$L^{\mathrm{B}}_{\mathrm{lim-DMS}} = \min\left(L^{\mathrm{B}}_{\mathrm{lim}}, \frac{\mathrm{DMS}}{\mathrm{DMS} + K_{\mathrm{DMS-bac}}}\right) \quad (17)$$

$$L^{\mathrm{B}}_{\mathrm{PAR}} = \min\left(1., \max\left(0.66, 1. - \left(\frac{\mathrm{PAR}}{\mathrm{PAR}_{\mathrm{max}}}\right)^{6} + 0.18\right)\right) \quad (18)$$

The parameterization in Eq. 16 is similar to the formulation adopted in PISCES to compute the remineralization rate of DOM (see Eq. 21 in Aumont and Bopp 2006). The rate constant $\lambda^{\mathrm{B}}_{\mathrm{DMS}}$ for bacterial consumption of DMS is set to 0.2 day^{-1}, which is in the low end of the range estimated by Kieber et al. (1996) for the equatorial Pacific (0.2–0.6 day^{-1}). The limitation of bacterial activity $\left(L^{\mathrm{B}}_{\mathrm{lim-DMS}} * L^{\mathrm{B}}_{\mathrm{PAR}}\right)$ was taken from Vogt et al. (2010) (their Eqs. 10 and 11). The temperature dependence, b^{T}, is based on the power law of Eppley (1972) for phytoplankton. $\mathrm{B}_{\mathrm{DMS}}$ is a bacterial DMS coefficient currently set to 0.33 (Vogt et al. 2010). While PISCES does not explicitly model bacterial biomass, it is estimated as a linear combination of the zooplankton biomass terms (B = 0.7 (Z + 2 M) min(1, 120/z)) where Z and M are the micro- and meso-zooplankton concentrations, respectively, and z is the depth. This relationship has been constructed from a version of PISCES that included an explicit description of the bacterial biomass (see Aumont and Bopp 2006).

The photochemical loss rate of DMS is a function of PAR and nitrate (NO_3) concentration. For the DMS photolysis associated with PAR, we adopted the parametrization proposed by Archer et al. 2004 (their Eq. 12). Hence,

$$\lambda^{\mathrm{PAR}}_{\mathrm{DMS}} = f_3 * \frac{\mathrm{PAR}}{\mathrm{PAR} + h_1} \quad (19)$$

where f_3 is the maximum rate of photolysis of DMS to dissolved organic carbon (DOC). We also include the impact of NO_3 on the photochemical loss processes affecting DMS as suggested by Bouillon and Miller (2004). This results in the following empirical parameterization:

$$\lambda^{\mathrm{NO_3}}_{\mathrm{DMS}} = \max(L^{\mathrm{DMS}}_{\mathrm{NO_3}}, 0.01) \quad (20)$$

where

$$L^{\mathrm{DMS}}_{\mathrm{NO_3}} = [\mathrm{NO_3}] / \left(K^{\mathrm{DMS}}_{\mathrm{NO_3}} + [\mathrm{NO_3}]\right)$$

where in the Michaelis–Menten function for NO_3, the half saturation constant $\left(K^{\mathrm{DMS}}_{\mathrm{NO_3}}\right) = 10$ μM.

For ventilation to the atmosphere, the gas exchange coefficient, kg, is computed using the relationship as per Wanninkhof (1992) and the Schmidt number for DMS calculated following the formula given by Saltzman et al. (1993). At present, estimates for kg vary by a factor of 2, and the uncertainty increases with increasing wind speed (Vogt and Liss 2009; Elliott 2009).

Experimental design

Here we used the global configuration of NEMO–PISCES with a resolution of 2° × 0.5 to 2° and 31 vertical levels forced by an ocean circulation generated from climatological atmospheric forcings (Aumont et al. 2008). Following a spin up of many thousands of years we conducted short term sensitivity experiments for less than 5 years in order to capture the instantaneous response of the ocean's DMS system to change, rather than have the response complicated by the lateral and downstream effects that would be present in longer term integrations when nutrient limitation is perturbed (e.g., Tagliabue et al. 2008). In this way, we capture the direct effect of changes to bacterial nutrient limitation on DMS cycling, rather than the impacts associated with the modulation to nutrient recycling and thus phytoplankton growth that would also impact DMS cycling in longer term sensitivity experiments.

Results

It is clear that the biogeographic provinces are considerably less homogeneous in terms of Chl (Fig. 1) or POC concentrations (data not shown) than the cores of the subtropical gyres selected in the study of Morel et al. (2010). Moreover, the core of the North Atlantic subtropical gyre (South–Sargasso Sea) belongs to two different provinces (NASW and NATR). Hence, it is important to measure how the conclusions of our study of the dynamics of DMS in the most oligotrophic subtropical zones of the global ocean are affected by the use of different DMS datasets (i.e., discrete or climatological DMS data).

Spatial variability of the 'summer DMS paradox' assessed from climatological data

Global features

Figure 3 examines the spatial variations in the intensity of the 'summer DMS paradox' as calculated from the normalized levels of climatological monthly DMS concentrations to those of Chl (upper panel) or POC (bottom panel) for the months of August and February. Since POC exists in varying proportions to Chl, each measure of the 'summer DMS paradox' exhibits different trends in the Northern Hemisphere. There are no major differences in maximum DMS-to-Chl levels between the subtropical western North Pacific, the subtropical North Atlantic and the Mediterranean Sea. In terms of DMS-to-POC ratio, the subtropical North Atlantic is characterized by maximum levels about half of those observed in the two other basins. Thus the maximum intensity of the 'summer DMS paradox' is weaker in the Atlantic than in the other oceanic basins and the Mediterranean Sea. In particular, both climatological data sets suggest that the Indian South Subtropical Gyre is a better archetype for the 'summer DMS paradox' than the Sargasso Sea. It is also notable that a strong decoupling between DMS, and Chl or POC concentrations, also occurs off the Weddell Sea.

'Province based' approach: regional features in the subtropical Longhurst's biogeographic zones

The climatological monthly concentrations of DMS, Chl and POC have been spatially averaged over 10 biogeographic provinces of Longhurst (1998), with seven of them located in the Northern Hemisphere. These monthly quantities are displayed in Fig. 4 together with the corresponding DMS-to-Chl and DMS-to-POC ratios. For a detailed discussion of features in monthly regional mean climatology of DMS concentrations, the reader is referred to the paper of Lana et al. (2011). In the low and temperate latitudes of the Northern and Southern Hemispheres, DMS concentrations follow strong seasonal patterns with winter lows and summer highs except in the provinces NATR, NPTW and WARM (Fig. 4a, b). The WARM region follows a seasonal pattern with much higher DMS concentrations in winter despite little variation in Chl concentrations. This results in a very unusual seasonal pattern in DMS-to-Chl and DMS-to-POC ratios that is highly dissimilar to the seasonal trends in the provinces NASW and MEDI (Fig. 4g, i). Climatological data reveal that the 'summer DMS paradox' is of higher amplitude in MEDI than elsewhere in the Northern Hemisphere and also that it takes place in all subtropical provinces of the Southern Hemisphere, but with variable intensity that is highest in ISSG and lowest in SATL (Fig. 4g–j). The 'summer DMS paradox' in NASW and SPSG look very similar. Hence, according to our 'province based' approach, the 'summer DMS paradox' is widespread in subtropical oligotrophic waters.

'Station based' approach of 'summer DMS paradox' and associated physical and biogeochemical variables

Absolute and relative monthly DMS concentrations

The data used (1,427 DMS surface seawater concentration measurements (Table 1) plotted as red dots in Fig. 1) to investigate the monthly variations in DMS concentrations in the most oligotrophic subtropical zones of the global ocean (see the white boxes in Fig. 1) are solely taken from the Global Surface Seawater DMS Database (http://saga.pmel.noaa.gov/dms/). Data were averaged in each zone according to the sampling month (Fig. 5a) and normalized to climatological monthly concentrations of Chl and POC (Fig. 5b–c). Summer DMS mean levels in Md and S-ext. are similar. If we use P as a comparison with S-ext., we find that the levels across the subtropical North-Atlantic are markedly different in spring and summer. In summer, there is also a two- to threefold difference in DMS concentration between sites S-ext. and E-ext., and levels in site B are about half of those in site E-ext. Hence, during the summer the highest contrast is found between the sites B and S-ext. It is worthy to note here that monthly climatological DMS data averaged in the Longhurst's static biogeographic provinces (Fig. 4a, b) and monthly DMS data averaged in the core of the subtropical oligotrophic zones (Fig. 5a) provide distinct pictures. This probably results from the interpolation/extrapolation/substitution techniques applied to project the discrete concentration data onto a first guess field based on Longhurst's biogeographic provinces. It highlights how local dynamics can be 'averaged out' in climatology construction at regional scales. The E-ext. zone is

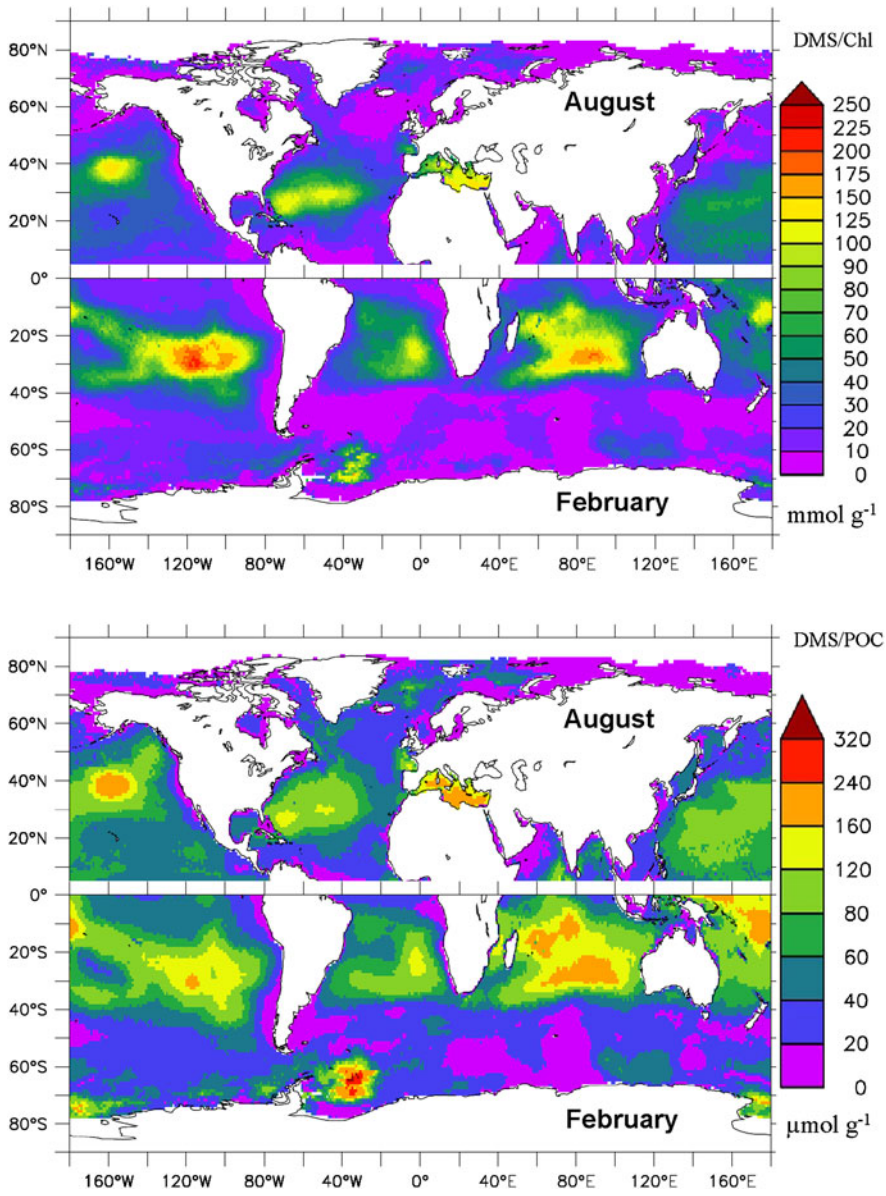

Fig. 3 Climatological monthly maps of DMS-to-Chl (*upper panel*, mmol g^{-1}) and DMS-to-POC (*bottom panel*, µmol g^{-1}) ratios for August (NH summer) and February (SH summer). Both ratios measure the spatial variability of the 'summer DMS paradox' (Simó and Pedrós-Alió 1999)

ambiguous as to whether a 'summer DMS paradox' exists there. Indeed, the DMS-to-Chl ratios calculated in mid and late summer in E-ext. (February–March) and S-ext. (August–September) are roughly similar (Fig. 5b). In late spring and early summer (December–January in the SH and June–July in the NH), the ratio in E-ext. is about half that in S-ext. When the intensity of the 'summer DMS paradox' is measured using DMS-to-POC ratios, the results are less ambiguous. It appears that the 'summer DMS paradox' is more important in S-ext. and Md than in E-ext. and B.

Physical and chemical oceanic variables (MLD, k_g, SRD PAR and UV, $\Xi^{MLD}(UV)$)

Monthly values extracted or calculated from climatologies are shown in Fig. 6. Here, we focus on summer patterns.

DMS sea-to-air transfer velocities show little differences between sites with the exception of area H where wind speeds are generally higher than in the other regions (Fig. 6b). Shallower mixed layer depths are observed in S-ext., Md and P (<30 m, Fig. 6a).

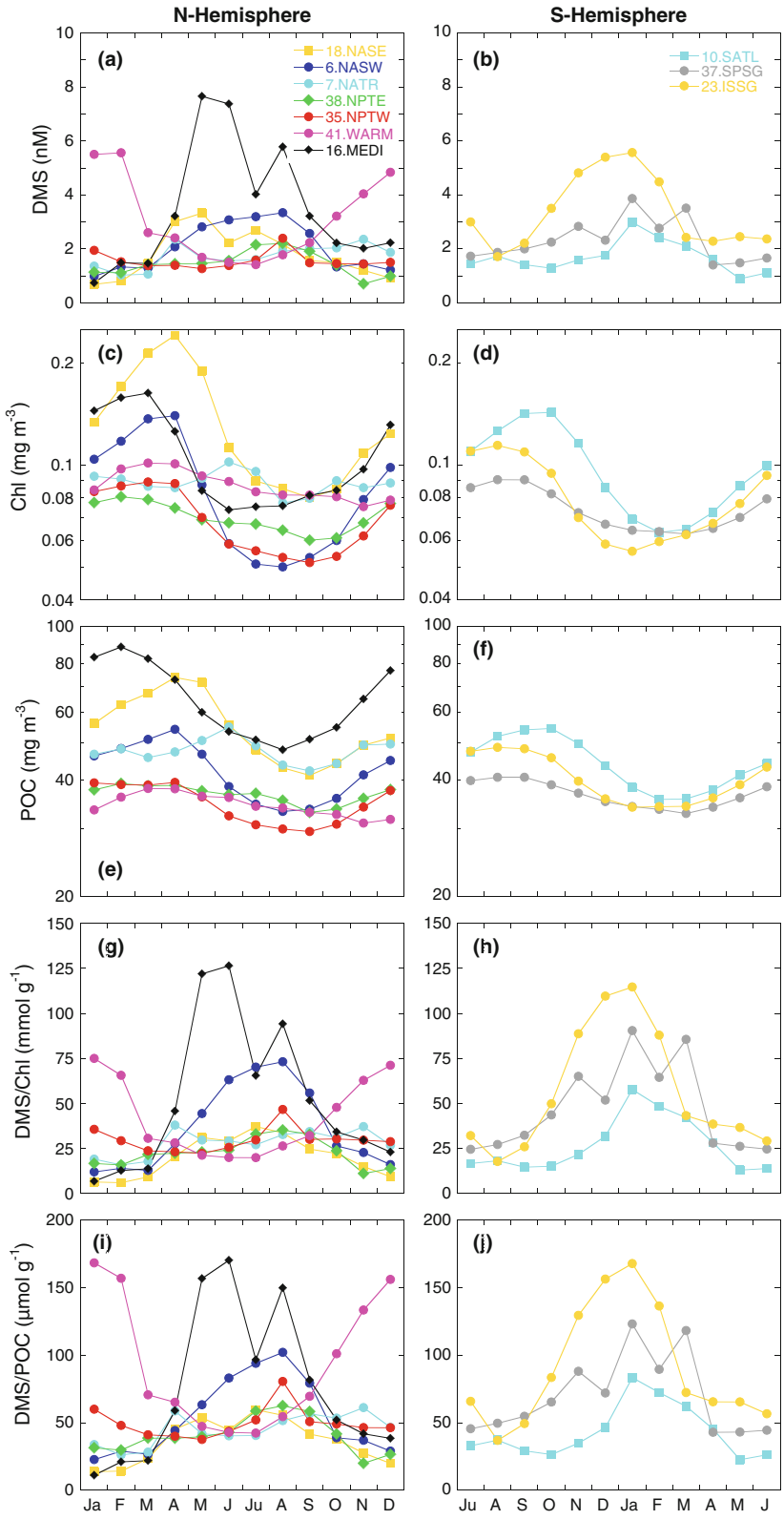

Fig. 4 Climatological annual cycles of averaged **a**, **b** DMS (Lana et al. 2011), **c**, **d** corrected Chl (Morel and Gentili 2009) and **e**, **f** POC (Duforêt-Gaurier et al. 2010) concentrations within the 10 Longhurst static biogeographic provinces (see Table 1 for the meaning of acronyms and reference numbers). For each region studied, the **g**, **h** DMS-to-Chl and **i**, **j** DMS-to-POC ratios were first calculated for the 1° × 1° pixels of the spatial grid corresponding to the region. Then, the spatial average for each region was computed. Both ratios measure the amplitude of the 'summer DMS paradox' (Simó and Pedrós-Alió 1999). The month scale begins with January for the Northern Hemisphere (*left panels*), and in July for the Southern Hemisphere (*right panels*). Note that Chl and POC concentrations are plotted on a log scale

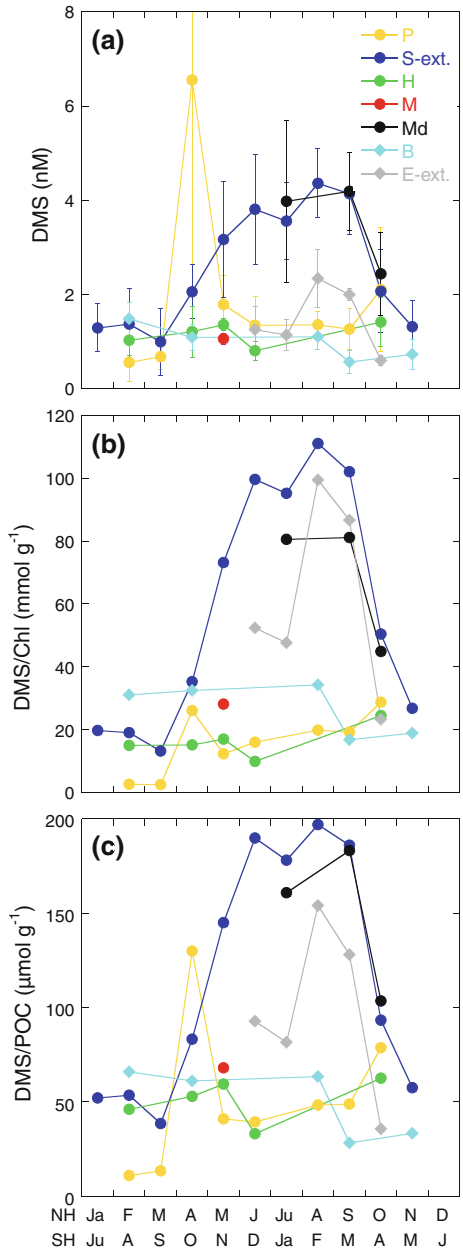

Fig. 5 Seasonal variations in monthly averaged DMS surface seawater concentrations in the most oligotrophic subtropical zones of the global ocean (**a**). The *vertical bars* correspond to ±1 standard deviation computed for each month and express the combined spatial and year-to-year variability of the monthly mean values inside each zone. Seasonal variations in monthly averaged DMS surface seawater concentrations normalized to monthly climatological Chl and POC concentrations (**b**, **c**). Note that site "P" (off Portugal) is not within the core of an oligotrophy zone and is used here for comparison

The influence of MLDs on mixed layer SRDs is obvious. In the UV domain, the highest SRDs are found in Md (Fig. 6c). SRDs in S-ext. and E-ext. are almost identical and are significantly higher than in B. Lower SRDs are found in P, M and H.

In the PAR domain, mixed layer SRDs were calculated from field measurements of irradiance, SST and light attenuation that coincide geographically and temporally with the DMS records. Therefore, we provide discrete SRD data in the PAR domain with units W m^{-2} as per Vallina and Simó (2007) together with the number of vertical profiles used for the determinations. SRDs were 75.1 ± 20.2 W m^{-2} ($n = 41$), 80.4 ± 6.7 W m^{-2} ($n = 35$), 91.9 ± 8.9 W m^{-2} ($n = 13$) and 43.8 ± 17.6 W m^{-2} ($n = 74$) in S-ext., Md, E-ext. and P, respectively.

The UV photon absorption rate averaged over the mixed layer was similar at all sites during summer, with maximum rates observed at site B (Fig. 6d). The reason for this similarity is essentially twofold. First, all study sites are typically exposed to a comparable level of incident UV irradiance during summer (see Fig. 3A, C in Fichot and Miller 2010 for summer values of incident irradiance in the Northern and Southern Hemisphere, respectively). Second, the large majority (>80%) of all incident UV photons is generally absorbed within the mixed layer, even in the subtropical gyres during summer when UV diffuse attenuation is low and the mixed layer is shallow (Fichot and Miller 2010).

Biological oceanic variables

Phytoplankton pigment-based size classes were used to document the structure of the phytoplankton community in each oligotrophic zone (Fig. 7). While total Chl *a* (TChl *a*) is a universal proxy for all phytoplanktonic organisms, accessory pigments measured by high performance liquid chromatography (HPLC) are specific to phytoplankton groups. Their respective proportion to TChl *a* can thus be used as a proxy for community composition. Here, we used the pigment grouping method recently improved by Uitz et al. (2006). Seven pigments are used as biomarkers of several phytoplankton taxa. Specific pigments and classes are described in Uitz et al. (2006), see their Table 2. These taxa are then grouped into three size classes (micro-, nano-, and picophytoplankton (prochlorophytes and cyanophytes)) according to the

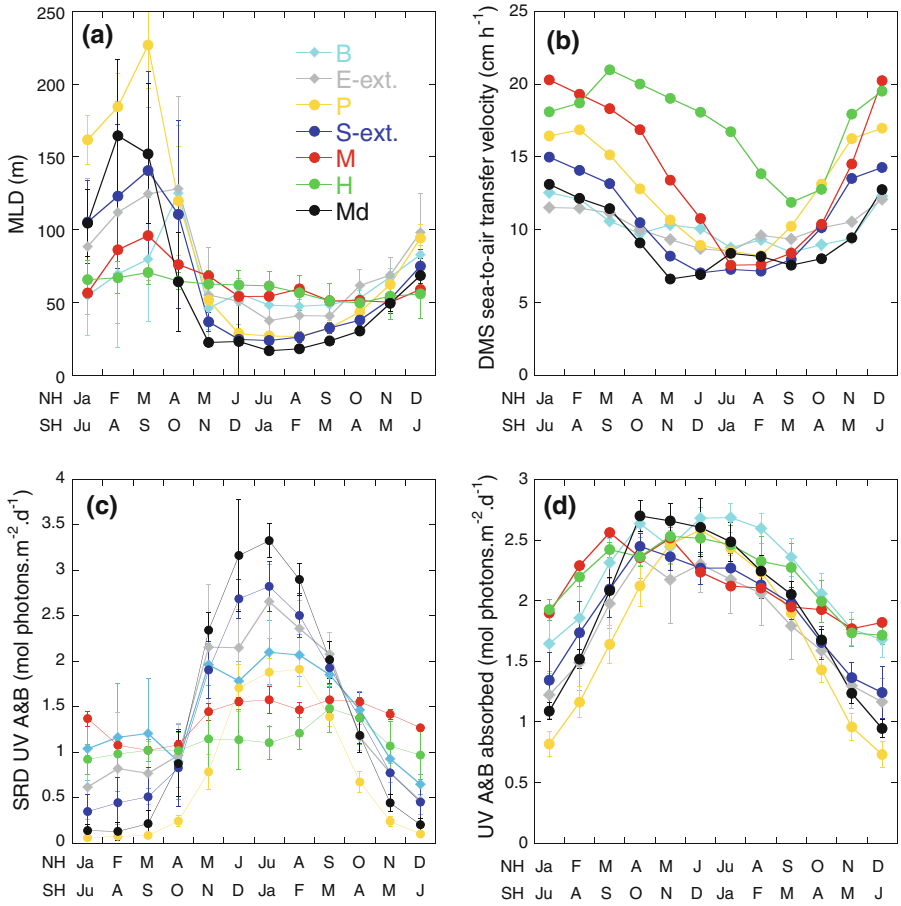

Fig. 6 Monthly climatological values of **a** the depth of the mixed layer, **b** the DMS sea-to-air transfer velocity of DMS, **c** the average incident UV downward scalar irradiance in the mixed layer (SRD UV), and **d** the average UV photon absorption rate in the mixed layer, averaged in each of the selected oligotrophic zones

average size of the cells. The fraction of each pigment-based size class with respect to the total phytoplankton biomass is calculated in each of the oligotrophic zones on a monthly basis. Unfortunately, some areas still remain poorly documented (e.g. E-ext., B and P; Fig. 7). In area H, the total phytoplankton biomass was generally higher than in the other regions and the phytoplankton community was dominated by picophytoplankton year-round (Fig. 7e). In area S-ext. during summer the dominant size class was nanophytoplankton. Picophytoplankton and nanophytoplankton were the dominant classes in the oligotrophic system Md. Summer data in E-ext. and B are lacking but the late spring data show that picophytoplankton and nanophytoplankton are the dominant classes.

The PHYSAT tool provides a way to trace the dominant phytoplankton populations from space at an unprecedented scale (Alvain et al. 2008). The PHYSAT algorithm, applied to the SeaWiFS daily L3-binned GAC data archive, identifies the following dominant phytoplankton groups in surface waters: Prochloroccocus (PRO), Synechococcus (SYN), nanoeukaryotes (NANO), Phaeocystis-like (PHAEO), coccolithophores (COC), and diatoms (DIAT). Climatological (1998–2006) monthly phytoplankton group dominance (PGD) data were used to corroborate the phytoplankton pigment-based size classes presented above. The main features in PGD in the Northern Hemisphere in summer (August) were: (1) SYN dominated in H and M, and (2) PRO and NANO dominated in S-ext. (Fig. 8a). SYN dominated in the areas E-ext., B and I in summer (February) in the Southern Hemisphere (Fig. 8b).

The adaptation of phytoplankton communities to extreme optical conditions (deep blue waters) can be investigated through the use of the photoprotection index PI = (Diadinoxanthin + Diatoxanthin)/[TChl *a*]. Diadinoxanthin and diatoxanthin, also measured by HPLC, are non-photosynthetic pigments produced by various phytoplankton taxa (mainly micro- and

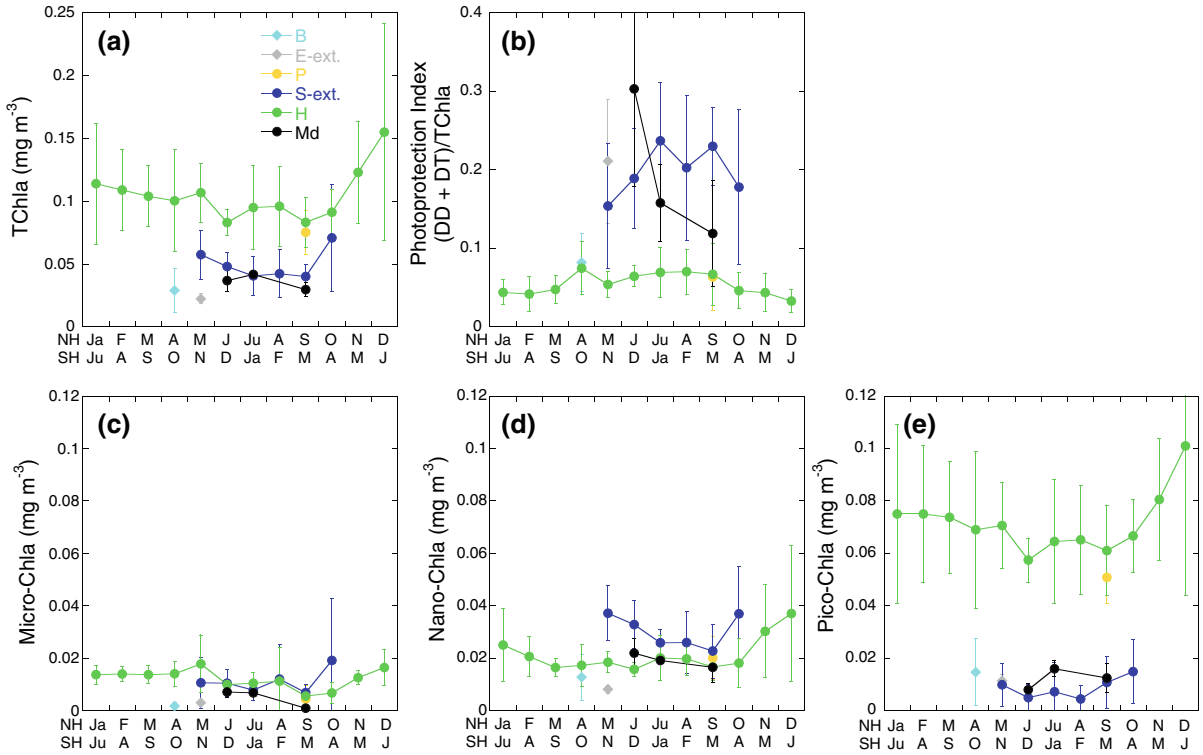

Fig. 7 Total phytoplankton biomass (**a**), light adaptation of phytoplankton (**b**) and phytoplankton pigment-based size classes (**c** micro-, **d** nano- and **e** picophytoplankton) in each oligotrophic zone investigated

nanophytoplanktion). They act to prevent photoinhibition and reactive oxygen species production. Hence, PI rather measures the light adaptation of micro- and nanophytoplankton. The oligotrophic zones showing higher values of photoprotection index are S-ext., Md and E-ext. (Fig. 7b).

Dissolved inorganic phosphorus (DIP) concentrations and turnover times (a measure of phosphate limitation), were gathered from the literature (Table 2). In S-ext. during summer, DIP concentrations in surface waters are 2–5 nM (Lomas et al. 2010). They are also in the low nM levels in Md where the depth of the 50 nM isoline is deeper than 150 m (Van Wambeke et al. 2002). In subtropical and intertropical Atlantic surface waters, DIP levels at 25 m are considerably higher (i.e. tens to hundreds of nM; Mather et al. 2008). In E-ext., DIP levels are over 200 nM (Moutin et al. 2008). Areas S-ext. and Md display extremely short turnover times in DIP (5 h and 1.2 ± 0.5 h; Moutin et al. 2008, respectively) as compared to E-ext. and the north-eastern Atlantic area P (5589 ± 1472 and 168 ± 110 h; Moutin et al. 2008, respectively). Nutrient limitation has also been assessed from enrichment experiments. The north-western Atlantic and the eastern Mediterranean Sea are areas where phytoplankton and bacterial growth is limited by phosphate availability (Wu et al. 2000; Van Wambeke et al. 2002) while nitrogen is the limiting nutrient in area E-ext. (Van Wambeke et al. 2008). According to Mather et al. (2008), the South Atlantic subtropical gyre is not phosphate-limited. These authors highlighted the asymmetry of dissolved organic phosphorus (DOP) cycling in the North and South Atlantic Ocean subtropical gyres and interpreted it as a consequence of enhanced nitrogen fixation in the North Atlantic Ocean, which forces the system towards phosphorus limitation.

'Model based' approach to DMS dynamics

Data obtained from satellite imagery by SeaWiFS (reprocessed by Morel et al. 2010) offer the means to validate the surface distribution of chlorophyll as

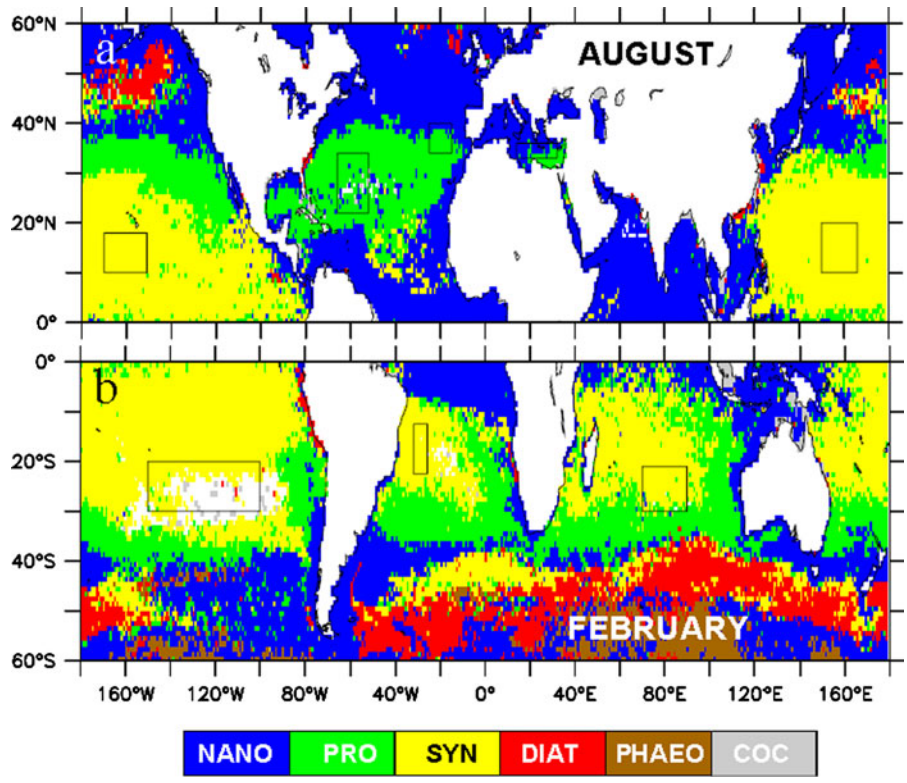

Fig. 8 Dominant phytoplankton groups for August (**a**) and February (**b**) from PHYSAT climatological composites (1998–2006, Alvain et al. 2008). Dominant phytoplankton groups are: Nanoeucaryotes (NANO), Prochloroccocus (PRO), Synechococcus (SYN), diatoms (DIAT), Phaeocystis-like (PHAEO) and coccolithophores (COC)

predicted by the PISCES model. Figure 9 shows the yearly mean, climatological, satellite-derived (a, SeaWiFS) and modelled distributions (b, PISCES) of chlorophyll at the surface. The satellite provides average values for the upper 10–20 m of the ocean that are directly comparable to the model output. The main observed patterns are reproduced by the model. Very low concentrations of Chl are found in the oligotrophic subtropical gyres. They drop below 0.05 mg Chl m^{-3} both in the model and in the observations. In the equatorial Pacific Ocean the predicted chlorophyll concentrations are slightly overestimated. The patterns observed in the latitude-time (Hovmøller) maps confirms that the model is able to closely simulate the spatial and seasonal variations in Chl (Fig. 9c, d). In terms of DMS, the model simulation and the annual climatological map constructed from Lana et al. (2011) diverge mostly in how they represent DMS structures at mid- to high-latitudes (Fig. 9e, f). Moreover, the climatology of Lana et al. (2011) suggests zonal patterns with DMS summer maxima coinciding with Chl maxima at high SH latitudes (compare Fig. 9g and c). The coincidence with Chl is reduced at mid- to high-NH latitudes. The model produces zonal DMS fields that do not follow closely those of Chl almost everywhere (compare Fig. 9h and d). Moreover, at mid- to high-latitudes, simulations and climatological data of Lana et al. (2011) differ markedly (compare Fig. 9g and h). The results of the sensitivity experiment in the subtropical oligotrophic zones will be presented in the discussion.

Discussion

In their paper dated 2008, Vila-Costa et al. proposed an explanation of the links from SRD to the biogeochemical cycle of DMS: "In highly irradiated waters typical of summer conditions, stronger stratification of the water column favours high DMSP-producing phytoplankton, and high UV irradiances in shallow mixed layers generate high UV radiation doses for plankton that may inhibit the consumption of DMSP and DMS by bacteria and enhance the anti-oxidative responses of phytoplankton, all resulting in higher DMS production than consumption." Our work aims

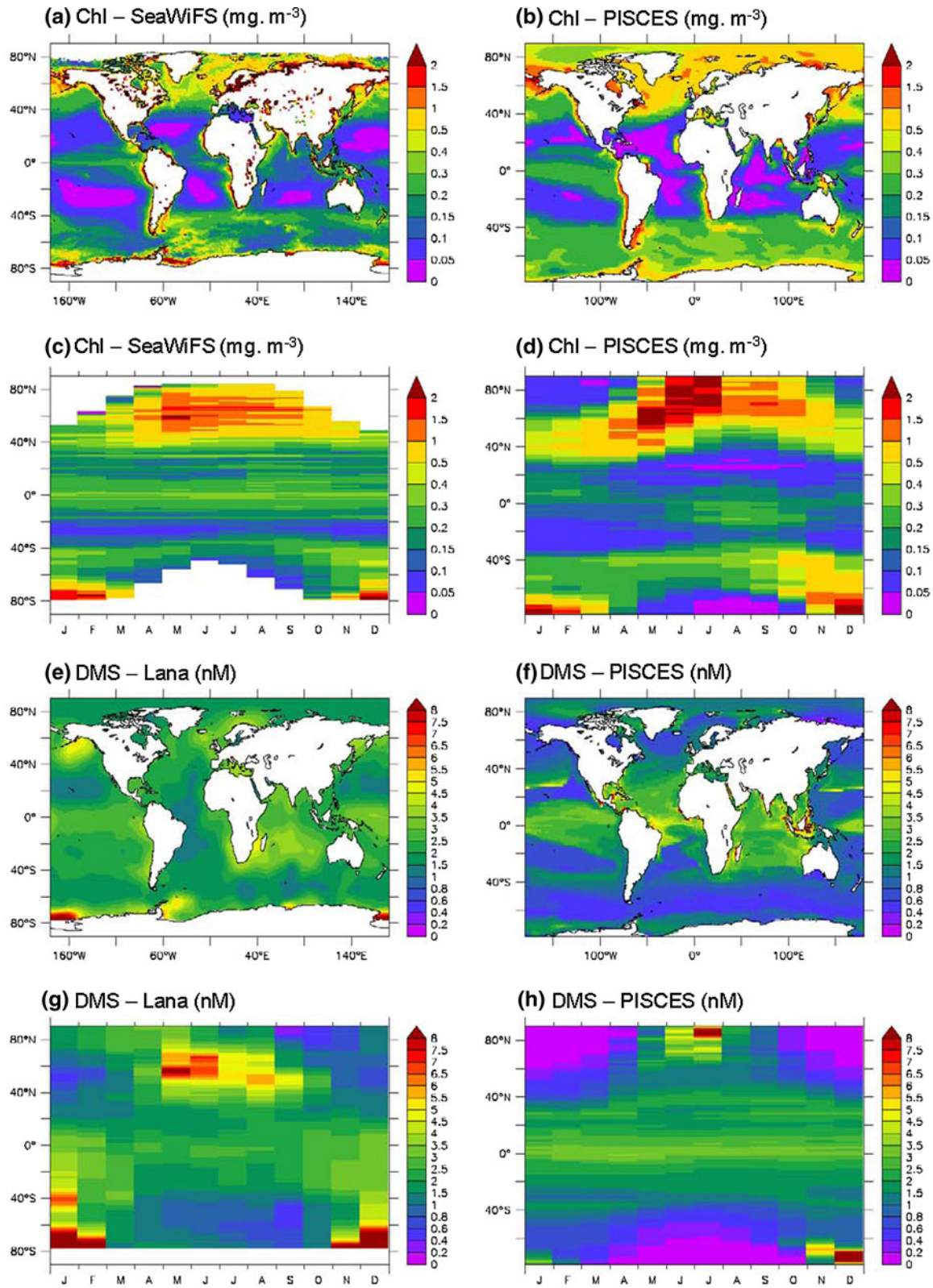
(a) Chl – SeaWiFS (mg. m-3)
(b) Chl – PISCES (mg. m-3)
(c) Chl – SeaWiFS (mg. m-3)
(d) Chl – PISCES (mg. m-3)
(e) DMS – Lana (nM)
(f) DMS – PISCES (nM)
(g) DMS – Lana (nM)
(h) DMS – PISCES (nM)
80°N
40°N
0°
40°S
80°S
160°W
60°W
40°E
140°E
100°W
0°
100°E
J F M A M J J A S O N D
2 1.5 1 0.5 0.4 0.3 0.2 0.15 0.1 0.05 0
8 7.5 7 6.5 6 5.5 5 4.5 4 3.5 3 2.5 2 1.5 1 0.8 0.6 0.4 0.2 0

◀ **Fig. 9** Comparison of field observations (*left panels*) and computer simulations performed using the PISCES model (*right panels*). The four *upper panels* (**a**–**d**) show maps of annual mean Chl concentration (mg m^{-3}) and latitude-time (Hovmøller) maps of Chl (Morel et al. 2010). The four *lower panels* (**e**–**h**) are for DMS concentrations (nM; Lana et al. 2011)

at testing this causal link in other oligotrophic subtropical zones of the global ocean than the Sargasso Sea which is often considered as an archetype for oligotrophic regimes but is certainly not the bluest sea (Morel et al. 2010). Indeed, the Sargasso Sea, as well as the Mediterranean Sea, are not as blue as it could be expected from their low Chl level, essentially because of a relative CDOM excess (Morel and Gentili 2009; Morel et al. 2010). Based on the high correlation between DMS and SRD at local scales (Vallina and Simó 2007), we expected that the clearest and the most oligotrophic waters of all the subtropical gyres, i.e. the South Pacific Gyre (Morel et al. 2010), would display the highest DMS surface levels. SRDs in the PAR domain, for which a new method of calculation based on field observations of all its components is proposed here, are indeed higher than elsewhere (Fig. 10). However, we find that DMS concentrations are two- to threefold lower in the South Pacific Gyre than in the Sargasso or the eastern Mediterranean Seas. Moreover, DMS levels in E-ext. and P are roughly similar whereas SRDs in P are about twice as low as in E-ext. (see also data of Fig. 7 in Morel et al. 2010 for a representation of the annual cycle of SRD in the PAR domain in the zones E-ext. and P). DMS concentrations and SRDs in the UV domain are strongly correlated in zone S-ext. (Fig. 11a). At high SRDs, there is a better agreement in terms of DMS levels between the S-ext. and Md zones than between the former zone and E-ext. The linear relationship in the S-ext. zone is even more significant when DMS levels normalized to Chl or POC concentrations are plotted against SRD-UV (Fig. 11b, c). However, few data points from other subtropical zones fit in. Moreover, most data points lay below those regression lines. This is a pattern already noticed by Miles et al. (2009) in their Atlantic Ocean study of the relationship between total solar radiation dose and DMS (compare Fig. 11a (this work) with Fig. 2a in Miles et al. 2009). Overall, our observations provide evidence that the SRD in the PAR and UV spectral domains do not control DMS spatial variations in oligotrophic waters of the global ocean. The

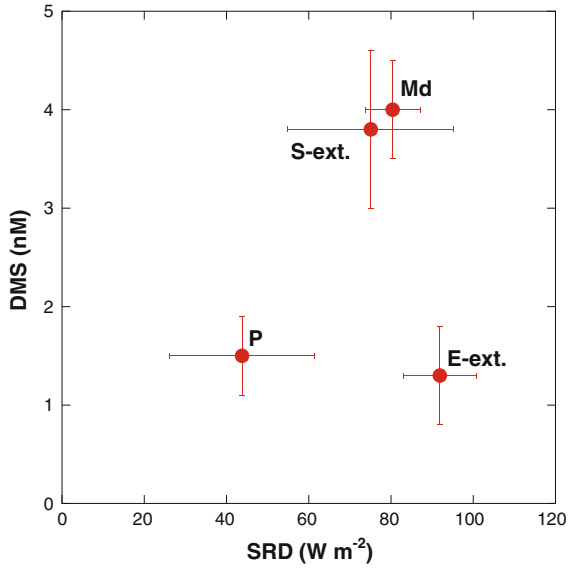

Fig. 10 Scatter diagram of averaged DMS sea surface concentrations in four selected zones plotted against SRD in the PAR spectral domain. In situ data for all of the components (MLD, irradiance and light attenuation) have been used to calculate SRDs

amplitude of the excess in DMS concentration relative to that of Chl or POC is probably modulated by other factors than the penetration of solar radiation in the sea. In other words, the causal link between SRD and DMS which relies on a series of laboratory and field observations (Dacey et al.1998; Aumont et al. 2002; Vallina and Simó 2007; Sunda et al. 2007) should be revised to integrate the fact that DMS-to-SRD, DMS-to-Chl, DMS-to-POC ratios and most likely DMS-to-DMSP ratios, differ from one oligotrophic ecosystem to another.

The influences of physico-chemical and biological variables on summer concentrations of DMS were investigated in the most oligotrophic subtropical zones of the global ocean. Unfortunately, very few DMS measurements have been made in the South Indian gyre and in the Mariana and Hawaii Islands zones during summer. Similarities and differences in terms of physical, chemical and biological variables between the S-ext. zone and other oligotrophic subtropical zones (Md, P, E-ext. and B) are summarized in Table 2. The S-ext. and Md zones display strong similarities in absolute or relative DMS concentrations, in physical properties and in biogeochemical regime: surface waters are highly stratified and DIP is

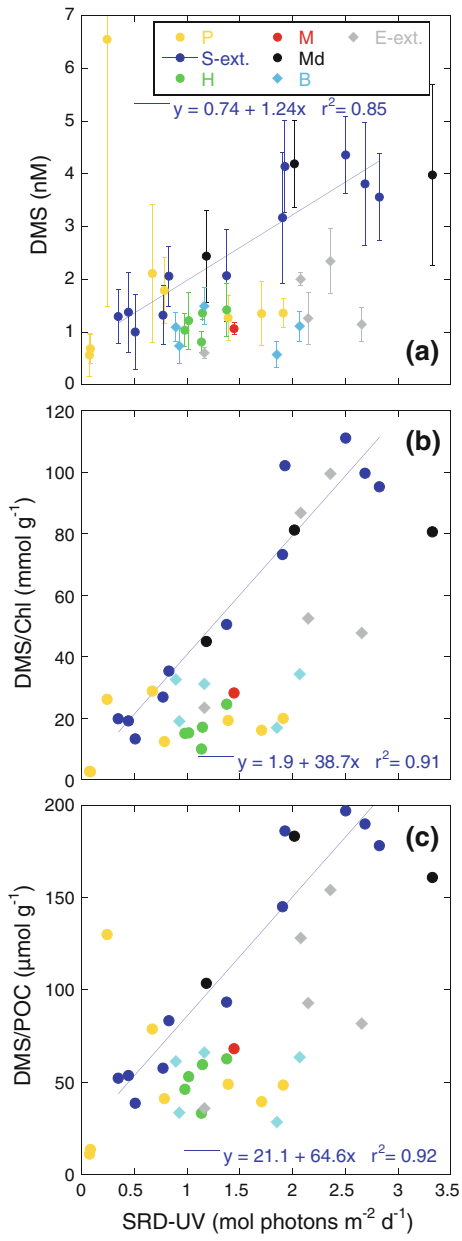

Fig. 11 Scatter diagrams of **a** averaged DMS sea surface concentrations and **b**, **c** averaged DMS concentrations normalized to Chl or POC concentrations, respectively, plotted against SRD in the UV spectral domain. Climatological data for all of the components (MLD, irradiance and light attenuation) has been used to calculate the SRDs. The regression lines (plotted in *blue*) are for the "S-ext." dataset. See Table 1 for the exact locations and meaning of the identifiers

depleted, nanophytoplankton make an important contribution to the phytoplankton community and are adapted to high irradiances, DIP turnover rates are extremely short (h) and phosphorous is the limiting nutrient for phytoplankton and bacterial growth. In the P zone, a highly stratified but not phosphorous-depleted area exhibiting DIP turnover rates of hundreds of hours, nanophytoplankton makes a smaller contribution to the phytoplankton community and does not show high levels of photoprotection index, probably as a result of lower surface irradiance and SRD. The Southern Hemisphere zone E-ext. is considerably less stratified than the former three zones and is distinct in terms of phytoplankton composition and nutrient regime. The dominant phytoplankton group is SYN and the limiting nutrient of phytoplankton and bacterial growth in early summer is nitrogen. The B zone is clearly not phosphate limited (Mather et al. 2008). If we remove the site "P" from the analysis (because of the lack of permanent oligotrophy there, but one should remind that site S-ext. exhibits no permanent oligotrophy too), none of the variables taken individually can account for the differences in absolute and relative concentrations of DMS. Indeed, the Northern and Southern Hemisphere zones are distinct in terms of (1) water stratification (higher in the NH), (2) phytoplankton taxa (more nanophytoplankton in NH), and (3) nutrient regime because P-limitation of phytoplankton and bacterial growth characterizes the NH sites S-ext. and Md. It is impossible to evaluate which one of the three variables is dominant. However, the lower DMS levels measured in summer in site "P" than in sites "S-ext." and "Md" cannot result from changes in water stratification or phytoplankton taxa because both variables are very similar. Conversely, the DIP concentrations and turnover times are sufficiently different to suggest that the nutrient regime is the determining variable. The causal link between SRD and high DMS levels in summer would be valid only in phosphorus-limited oligotrophic waters.

Phosphorus is an obligate requirement for growth of all organisms (Van Mooy et al. 2009). The authors also demonstrated that phytoplankton have an advantage over heterotrophic bacteria for growth in phosphorus-limited oligotrophic waters, even if primary production remains close to its lowest values in such environments. The fundamental biochemical mechanism allowing phytoplankton growth in phosphorus-limited environments would be the ability of phytoplankton to substitute membrane phospholipids by sulphur- and nitrogen-containing lipids that are free of

phosphorus (Van Mooy et al. 2009). Consequently, in phosphorus-limited environments, phytoplankton would maintain slow growth while heterotrophic bacterial growth would be much more severely limited by P-depletion. This would result in higher DMS production than consumption and favour a build-up in DMS. The Northern Atlantic subtropical gyre and the Mediterranean Sea, which are subject to iron deposition from Saharan dust, are depleted in the nutrient phosphate, possibly as a result of iron-enhanced nitrogen fixation (Wu et al. 2000).

In this study, we use the PISCES ocean biogeochemical model to explore the relationship between phosphorus limitation and DMS production in oligotrophic subtropical waters. It is worth reminding here how the biogeochemical model deals with the limitation of phytoplankton and bacterial growth. PISCES parameterizes the limitation of phytoplankton and bacterial growth by nutrients under a Monod framework using Michaelis–Menten kinetics, whereby the half saturation constant for growth is used to calculate the proportion of maximum growth permitted by each nutrient in turn. The overall growth rate is then the product of either the light limitation term (for phytoplankton) or the DOC limitation term (for bacteria) and the limitation term for the most limiting nutrient. For bacteria Fe, PO_4 and NH_4, whereas for phytoplankton NO_3, NH_4, PO_4, Fe and (for diatoms) $Si(OH)_4$ are considered growth limiting nutrients. N_2 fixation is included in PISCES as a process that is assumed to result in the net production of reduced N under certain conditions, in short it is enhanced under high light, high temperature and low NO_3 conditions and its rate is further regulated by Fe or PO_4 limitation. The switch from phosphorus limited to non-limited conditions was solely applied in the DMS module. Variable sulfur-to-carbon ratios in phytoplankton, variable transfer efficiency from DMS precursor to DMS, and variable bacterial DMS-consumption rate are taken into account. This 'model based' approach shows that the DMS-to-Chl ratio can be heavily impacted by phosphorus limitation in the North Pacific, North Atlantic and most sectors of the Indian Ocean, as the comparison of Fig. 12b, d and a, c shows. The impact of phosphorus limitation extends in the South Atlantic along the South American coast but not in the core of the South Atlantic subtropical gyre (Fig. 12c). There is no sensitivity to phosphorus limitation in the core of the South Pacific gyre (compare Fig. 12d with c). Both the S/C ratio of nanophytoplankton and the DMSP-to-DMS conversion yield are markedly affected (up to $\sim -25\%$) when phosphorus non-limited conditions are used (Table 7). The nutrient stress factor of bacteria, which also controls bacterial removal of DMS (Eqs. 16, 17), is also heavily impacted by phosphorus limitation. MLD integrated monthly budgets ($\mu mol\ m^{-2}\ month^{-1}$) for August (Sargasso Sea) and February (South Pacific and South Atlantic gyres; see Fig. 12 for exact locations) drawn for the standard run and the sensitivity test are shown in Fig. 13. The DMS budget in the South pacific gyre remains unaffected by phosphorus limitation. In both cases, the removal of DMS by bacteria accounts for 90% of the total production (i.e. 90% of production is processed by bacteria). When phosphorus limitation is released in the Sargasso Sea, DMS production decreases from 160 to 100 $\mu mol\ m^{-2}\ month^{-1}$ and DMS removal increases from 56 to 72 $\mu mol\ m^{-2}\ month^{-1}$. As a consequence, only 35% of DMS production is processed by bacteria under phosphorus-limited conditions, whereas $\sim$ 75% of DMS production is processed by bacteria under phosphorus-replete conditions. In the South Atlantic gyre, the DMS budget is affected by P limitation but more marginally than in the North Atlantic gyre. Finally, model results show that the Indian south subtropical gyre is the sole SH area where 'strong summer paradox' takes place throughout the whole basin. This is consistent with the climatological analysis but remains to be confirmed from field observations in the core of this oligotrophic zone.

Summary and conclusions

The most oligotrophic subtropical zones of the global ocean have been compared with respect to their DMS, Chl and POC contents by using two different approaches to the 'summer DMS paradox'. The first approach documented the seasonal variations of absolute and relative concentrations of DMS in the corresponding Longhurst's static biogeographic provinces, using values extracted from a recently updated monthly climatology of DMS and monthly satellite composites of Chl and POC concentrations. DMS-to-Chl and DMS-to-POC ratios exhibited strong seasonal cycles in the North and South Atlantic gyres, the South

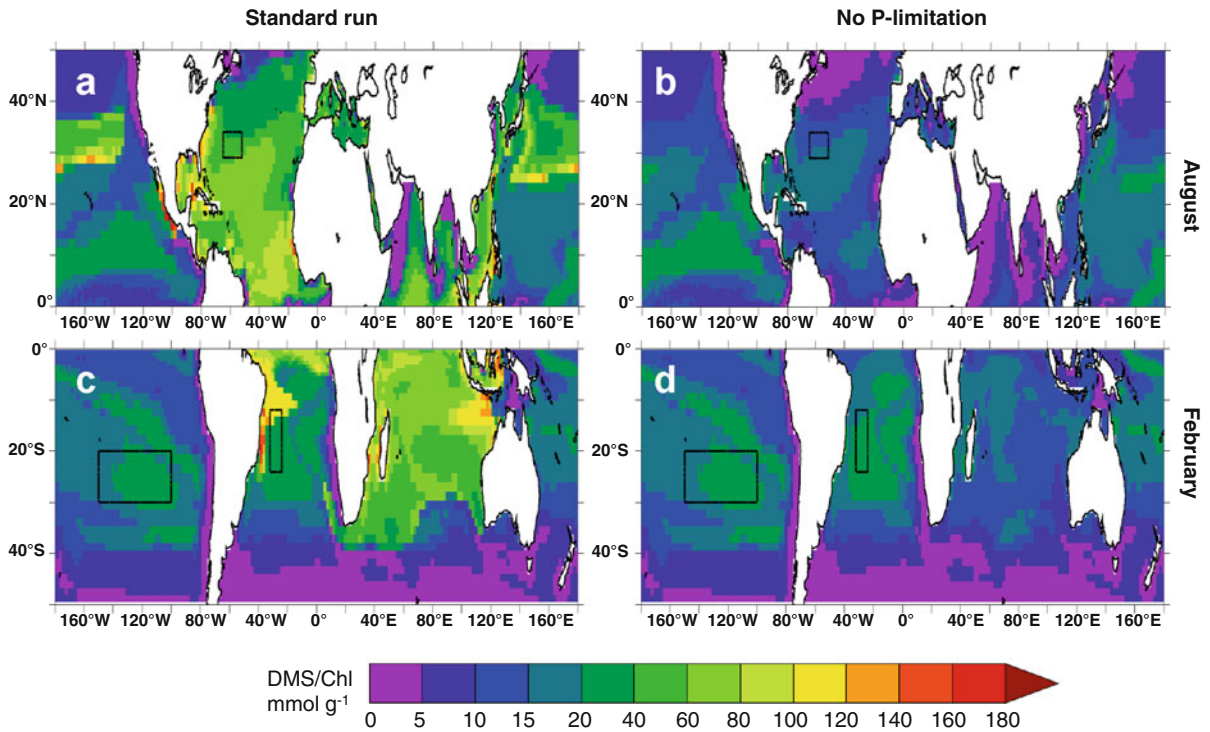

Fig. 12 Comparison of computer simulations performed using the PISCES model: with P limitation (standard run; *left panels* (**a**, **c**)), without P-limitation (*right panels* (**b**, **d**)). Results are shown for the summer months (August in NH and February in SH; *top and bottom rows*, respectively). *Black boxes* correspond to selected locations where DMS budgets were calculated (see text). A short run was performed to capture the immediate response of the DMS module to these changes rather than the longer term feedbacks mediated by ocean circulation. The simulation for the fourth year is presented here

Table 7 MLD averaged values of S/C ratio (units is mol - mol^{-1}) for nanophytoplankton, DMSP-to-DMS conversion yield (Y_S) and bacterial nutrients stress factor (L^B_{lim}) estimated using PISCES at selected locations: Sargasso Sea close to the BATS station, in the core of the South Pacific subtropical gyre and in the South Atlantic gyre (see black boxes in Fig. 12)

	Standard run (MLD averaged)	No P-limitation (%)
Sargasso Sea (BATS)	$S/C_{nano} = 0.030$	−17
	$Y_S = 0.59$	−24
	$L^B_{lim} = 0.008$	+8600
South Pacific gyre	$S/C_{nano} = 0.025$	0
	$Y_S = 0.47$	0
	$L^B_{lim} = 0.67$	0
South Atlantic gyre	$S/C_{nano} = 0.030$	−5
	$Y_S = 0.59$	−5
	$L^B_{lim} = 0.57$	+22

Relative changes of $S/C_{nano,}$ Y_S and L^B_{lim} averaged values for the sensitivity experiment (no P-limitation) relative to the standard run data are expressed in %. L^B_{lim} affects both Y_S and the bacterial consumption of DMS (λ^*_{DMS}, Eqs. 16 and 17)

Pacific gyre, the Indian south subtropical gyre as well as in the Mediterranean Sea, with maxima in summer and minima in winter. Thus, it appears that a 'summer DMS paradox' is a common feature in most oligotrophic subtropical biogeographic provinces. The second approach documented the monthly variations of absolute and relative concentrations of DMS in the cores of the most oligotrophic subtropical zones of the global ocean, using discrete values extracted from the Global Surface Seawater DMS Database and monthly satellite composites of Chl and POC concentrations since supporting Chl and POC data are not always available from this database. The sites located in the Northwestern Atlantic (S-ext.) and the eastern basin of the Mediterranean Sea (Md) exhibited two- to three-fold higher DMS levels in summer than in other NH and SH locations. The surface radiation dose (SRD) was calculated both in the PAR and UV spectral domains and its influence on absolute and relative concentrations of DMS was investigated through monthly and spatial variations. The influence of

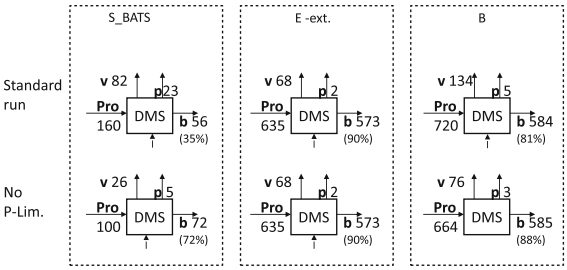

Fig. 13 DMS budgets drawn in the 3 selected zones Sargasso Sea-BATS (S_BATS), E-ext. and B (see Fig. 12 for printed locations). The computer simulations were performed using the PISCES model: with P limitation (standard run; *top row*), without P limitation (*bottom row*). Production and removal fluxes of DMS in units of μmol m^{-2} $month^{-1}$ were integrated vertically (MLD; 25, 43 and 50 m, S_BATS, E-ext. and B, respectively) and averaged in each zone for August (S_BATS) and February (E-ext. and B locations). (Pro) stands for DMS *pro*duction, (v) for *v*entilation to atmosphere, (p) for *p*hotodegradation and (b) for *b*acterial removal. The ratio of bacterial removal to DMS production is expressed in % and plotted between brackets below the bacterial removal fluxes

SRD on DMS was much less important outside the S-ext. and Md zones. The differences in absolute and relative concentrations of DMS between five oligotrophic sites were better accounted for by their nutrient regimes than by stratification or phytoplankton taxa. In other words, it appears that a strong 'summer DMS paradox' preferentially takes place in phosphorus-limited zones. A sensitivity experiment performed using a new version of the PISCES 3D model demonstrated the existence of a potential causal link between P limitation and the 'summer DMS paradox'.

Acknowledgments We are grateful to J.E. Johnson (JISAO, University of Washington) and T.S. Bates (PMEL, NOAA) for the maintenance and personal involvement in the Global Surface Seawater DMS Database. The authors also wish to thank each of the participants in the joint initiative of the SOLAS Integration project and the EU project COST Action 735 for providing an updated DMS climatology, with special thanks to the lead author A. Lana. A. Longhurst kindly provided the biogeographic provinces data. We would like to thank A. Morel and B. Gentili for sharing ocean color data. We are grateful to Dr. Scott Elliott and an anonymous reviewer for improvements to an earlier version of this manuscript. The model work was performed using HPC resources from GENCI-IDRIS (Grant 2009-010040 LSCE contribution 4662).

References

Alvain S, Moulin C, Dandonneau Y, Loisel H (2008) Seasonal distribution and succession of dominant phytoplankton groups in the global ocean: a satellite view. Glob Biogeochem Cycles. doi:10.1029/2007GB003154

Andreae MO (1990) Ocean–atmosphere interactions in the global biogeochemical sulfur cycle. Mar Chem 30:1–29

Archer SD, Smith GC, Nightingale PD, Widdicombe CE, Tarran GA, Rees AP, Burkill PH (2002) Dynamics of particulate dimethylsulphoniopropionate during a Lagrangian experiment in the northern North Sea. Deep-Sea Res Part II 49: 2979–2999

Archer SD, Gilbert FJ, Allen JI, Blackford J, Nightingale PD (2004) Modelling of the seasonal patterns of dimethylsulphide production and fate during 1989 at a site in the North Sea. Can J Fish Aquat Sci 61:765–787

Archer SD, Cummings DG, Llewellyn CA, Fishwick JR (2009) Phytoplankton taxa, irradiance and nutrient availability determine the seasonal cycle of DMSP in temperate shelf seas. Mar Ecol Prog Ser 394:111–124

Aumont O, Bopp L (2006) Globalizing results from ocean in situ fertilization experiments. Glob Biogeochem Cycles. doi: 10.1029/2005GB002591

Aumont O, Belviso S, Monfray P (2002) Dimethylsulfoniopropionate (DMSP) and dimethylsulfide (DMS) sea surface distributions simulated from a global threedimensional ocean carbon cycle model. J Geophys Res Oceans. doi: 10.1029/1999JC000111

Aumont O, Bopp L, Schulz M (2008) What does temporal variability in aeolian dust deposition contribute to sea-surface iron and chlorophyll distributions? Geophys Res Lett. doi:10.1029/2007GL031131

Belviso S, Caniaux G (2009) A new assessment in North Atlantic waters of the relationship between DMS concentration and the upper mixed layer solar radiation dose. Glob Biogeochem Cycles. doi:10.1029/2008GB003382

Bopp L, Aumont O, Belviso S, Blain S (2008) Modeling the effect of iron fertilization on dimethylsulfide emissions in the Southern Ocean. Deep-Sea Res Part II 35:901–912

Bouillon RC, Miller WL (2004) Determination of apparent quantum yield spectra of DMS photo-degradation in an in situ iron-induced Northeast Pacific Ocean bloom. Geophys Res Lett. doi:10.1029/2004GL019536

Bucciarelli E, Sunda WG (2003) Influence of CO_2, nitrate, phosphate, and silicate limitation on intracellular dimethylsulfoniopropionate in batch cultures of the coastal diatom Thalassiosira pseudonana. Limnol Oceanogr 48: 2256–2265

Cotner JB, Ammerman JW, Peele ER, Bentzen E (1997) Phosphorus-limited bacterioplankton growth in the Sargasso Sea. Aquat Microb Ecol 13:141–149

Dacey JWH, Howse FA, Michaels AF, Wakeham SG (1998) Temporal variability of dimethylsulfide and dimethylsulfoniopropionate in the Sargasso Sea. Deep-Sea Res Part I 45:2085–2104

de Boyer Montégut C, Madec G, Fischer AS, Lazar A, Iudicone D (2004) Mixed layer depth over the global ocean: an examination of profile data and profile-based climatology. J Geophys Res Oceans. doi:10.1029/2004JC002378

Derevianko GJ, Deutsch C, Hall A (2009) On the relationship between ocean DMS and solar radiation. Geophys Res Lett. doi:10.1029/2009GL039412

Duforêt-Gaurier L, Loisel H, Dessailly D, Nordkvist K, Alvain S (2010) Estimates of particulate organic carbon over the

euphotic depth from in situ measurements. Application to satellite data over the global ocean. Deep-Sea Res Part I 57:351–367
Elliott S (2009) Dependence of DMS global sea-air flux distribution on transfer velocity and concentration field type. J Geophys Res Oceans. doi:10.1029/2008JG000710
Eppley RW (1972) Temperature and phytoplankton growth in the sea. Fish Bull 70:1063–1085
Fichot CG, Miller WL (2010) An approach to quantify depth-resolved marine photochemical fluxes using remote sensing: application to carbon monoxide (CO) photoproduction. Remote Sens Environ 114:1363–1377
Fichot CG, Sathyendranath S, Miller WL (2008) SeaUV and SeaUVc: algorithms for the retrieval of UV diffuse attenuation coefficients from ocean color. Remote Sens Environ 112(4):1584–1602
Jerlov NG (1974) A simple method for measuring quanta irradiance in the ocean, Rep. 24. Inst. Fysik Oceanografi, Kobenhavens Universitet
Jerlov NG (1977) Classification of sea water in terms of quanta irradiance. J Cons Int Explor Mer 37(3):281–287
Jitts HR, Morel A, Saijo Y (1976) The relation of oceanic primary production to available photosynthetic irradiance. Aust J Mar Freshw Res 27:441–454
Kara AB, Rochford PA, Hurlburt HE (2003) Mixed layer depth variability over the global ocean. J Geophys Res Oceans. doi:10.1029/2000JC000736
Karsten U, Kück K, Vogt C, Kirst GO (1996) Dimethylsulfoniopropionate production in phototrophic organisms and its physiological function as a cryoprotectant. In: Kiene RP, Visscher PT, Keller MD, Kirst GO (eds) Biological and environmental chemistry of DMSP and related sulfonium compounds. Plenum, New York, pp 143–153
Katsaros K, Mcmurdie L, Lind R, DeVault J (1985) Albedo of a water surface, spectral variation, effects of atmospheric transmittance, sun angle and wind speed. J Geophys Res Oceans 90:7313–7321
Kettle AJ, Andreae MO, Amouroux D, Andreae TW, Bates TS, Berresheim H, Bingemer H, Boniforti R, Curran MAJ, DiTullio GR, Helas G, Jones GB, Keller MD, Kiene RP, Leck C, Levasseur M, Malin G, Maspero M, Matrai P, McTaggart AR, Mihalopoulos N, Nguyen BC, Novo A, Putaud JP, Rapsomanikis S, Roberts G, Schebeske G, Sharma S, Simo R, Staubes R, Turner S, Uher G (1999) A global database of sea surface dimethylsulfide (DMS) measurements and a procedure to predict sea surface DMS as a function of latitude, longitude, and month. Glob Biogeochem Cycles 13:399–444
Kieber DJ, Jiao JF, Kiene RP, Bates TS (1996) Impact of dimethylsulfide photochemistry on methyl sulfur cycling in the equatorial Pacific Ocean. J Geophys Res Oceans 101:3715–3722
Kiene RP, Linn LJ, Bruton JA (2000) New and important roles for DMSP in marine microbial communities. J Sea Res 43:209–224
Lana A, Bell TG, Simó R, Vallina SM, Ballabrera-Poy J, Kettle AJ, Dachs J, Bopp L, Saltzman ES, Stefels J, Johnson JE, Liss PS (2011) An updated climatology of surface dimethlysulfide concentrations and emission fluxes in the global ocean, Glob Biogeochem Cycles. doi:10.1029/2010GB003850
Langley L, Leaitch WR, Lohmann U, Shantz NC, Worsnop DR (2010) Contributions from DMS and ship emissions to CCN observed over the summertime North Pacific. Atmos Chem Phys 10:1287–1314
Lefèvre M, Vézina A, Levasseur M, Dacey JWH (2002) A model of dimethylsulphide dynamics for the subtropical North Atlantic. Deep-Sea Res Part I 49:2221–2239
Lomas MW, Burke AL, Lomas DA, Bell DW, Shen C, Dyhrman ST, Ammerman JW (2010) Sargasso Sea phosphorus biogeochemistry: an important role for dissolved organic phosphorus (DOP). Biogeosciences 7:695–710
Longhurst A (1998) Ecological geography of the sea. Academic, London
Madec G, Delecluse P, Imbard M, Levy C (1998) OPA8.1 ocean general circulation model reference manual. Notes du pôle de modélisation de l'IPSL
Mather RL, Reynolds SE, Wolff GA, Williams RG, Torres-Valdes S, Woodward ME, Landolfi A, Pan X, Sanders R, Achterberg EP (2008) Phosphorus cycling in the North and South Atlantic Ocean subtropical gyres. Nat Geosci 1:439–443
Miles CJ, Bell TG, Lenton TM (2009) Testing the relationship between the solar radiation dose and surface DMS concentrations using in situ data. Biogeosciences 6:1927–1934
Morel A, Berthon JF (1989) Surface pigments, algal biomass profiles, and potential production of the euphotic layer: relationships reinvestigated in view of remote-sensing applications. Limnol Oceanogr 34(8):1545–1562
Morel A, Gentili B (2009) The dissolved yellow substance and the shades of blue in the Mediterranean Sea. Biogeosciences 6:2625–2636
Morel A, Claustre H, Gentili B (2010) The most oligotrophic subtropical zones of the global ocean: similarities and differences in terms of chlorophyll and yellow substance. Biogeosciences 7:3139–3151
Moutin T, Karl DM, Duhamel S, Rimmelin P, Raimbault P, Van Mooy BAS, Claustre H (2008) Phosphate availability and the ultimate control of new nitrogen input by nitrogen fixation in the tropical Pacific Ocean. Biogeosciences 5: 95–109
Payne RE (1972) Albedo of the sea surface. J Atmos Sci 29:959–970
Polimene L, Archer SD, Butenschön M, Allen JI (this issue) A mechanistic explanation of the Sargasso Sea DMS "summer paradox". Biogeochemistry
Ruggaber R, Dlugi RA, Nakajima T (1994) Modelling of radiation quantities and photolysis frequencies in the troposphere. J Atmos Chem 18(2):171–210
Saltzman ES, King DB, Holmen K, Leck C (1993) Experimental determination of the diffusion coefficient of dimethylsulfide in water. J Geophys Res Oceans 98:16481–16486
Simó R, Pedrós-Alió C (1999) Role of vertical mixing in controlling the oceanic production of dimethyl sulphide. Nature 402:396–399
Stefels J, Steinke M, Turner S, Malin G, Belviso S (2007) Environmental constraints on the production and removal of the climatically active gas dimethylsulphide (DMS) and implications for ecosystem modelling. Biogeochemistry 83(1–3):245–275
Sunda W, Kieber DJ, Kiene RP, Huntsman S (2002) An antioxidant function for DMSP and DMS in marine algae. Nature 418:317–320

Sunda WG, Hardison R, Kiene RP, Bucciarelli E, Harada H (2007) The effect of nitrogen limitation on cellular DMSP and DMS release in marine phytoplankton: climate feedback implications. Aquat Sci 69:341–351

Tagliabue A, Bopp L, Aumont O (2008) Ocean biogeochemistry exhibits contrasting responses to a large scale reduction in dust deposition. Biogeosciences 5:11–24

Todd JD, Rogers R, Li YG, Wexler M, Bond PL, Sun L, Curson ARJ, Malin G, Steinke M, Johnston AWB (2007) Structural and regulatory genes required to make the gas dimethyl sulfide in bacteria. Science 315:666–669

Toole DA, Siegel DA (2004) Light-driven cycling of dimethylsulfide (DMS) in the Sargasso Sea: Closing the loop. Geophys Res Lett. doi:10.1029/2004GL019581

Uitz J, Claustre H, Morel A, Hooker S (2006) Vertical distribution of phytoplankton communities in open ocean: an assessment based on surface chlorophyll. J Geophys Res Oceans. doi:10.1029/2005JC003207

Vallina SM, Simó R (2007) Strong relationship between DMS and the solar radiation dose over the global surface ocean. Science 315:506–508

Van Mooy BAS, Fredricks HF, Pedler BE, Dyhrman ST, Karl DM, Koblızek M, Lomas MW, Mincer TJ, Moore LR, Moutin T, Rappe MS, Webb EA (2009) Phytoplankton in the ocean use non-phosphorus lipids in response to phosphorus scarcity. Nature 458:69–72

Van Wambeke F, Christaki U, Giannakourou A, Moutin T, Souvemerzoglou K (2002) Longitudinal and vertical trends of bacterial limitation by phosphorus and carbon in the Mediterranean Sea. Microbiol Ecol 43:119–133

Van Wambeke F, Bonnet S, Moutin T, Raimbault P, Alarcon G, Guieu C (2008) Factors limiting heterotrophic bacterial production in the southern Pacific Ocean. Biogeosciences 5:833–845

Vezina AF (2004) Ecosystem modelling of the cycling of marine dimethylsulfide: a review of current approaches and of the potential for extrapolation to global scales. Can J Fish Aquat Sci 61:845–856

Vila-Costa M, Kiene RP, Simó R (2008) Seasonal variability of the dynamics of dimethylated sulfur compounds in a coastal northwest Mediterranean site. Limnol Oceanogr 53(1):198–211

Vogt M, Liss PS (2009) Dimethylsulfide and climate. In: Le Quéré C, Saltzman ES (eds) Surface ocean—lower atmosphere processes. Geophysical Monograph Series, vol 198, pp 197–232

Vogt M, Vallina SM, Buitenhuis ET, Bopp L, Le Quéré C (2010) Simulating dimethylsulphide seasonality with the Dynamic Green Ocean Model PlankTOM5. J Geophys Res Oceans. doi:10.1029/2009JC005529

Wanninkhof R (1992) Relationship between wind speed and gas exchange over the ocean. J Geophys Res Oceans 97:7373–7382

Wu J, Sunda W, Boyle EA, Karl DM (2000) Phosphate depletion in the Western Atlantic Ocean. Science 289:759–762